

BENG ELECTRICAL AND MECHANICAL ENGINEERING



Reproducing the Vibration Environment of the SpaceX Hyperloop Test Track

April 23rd 2019

Author: Daniel Carbonell
Project Supervisor: Dr Enrico Mastropaulo

Personal Statement

This is a new project that I proposed and carried out from start to finish. Advice and suggestions on the models were given by my supervisor and second marker but the overall direction of the project was set by myself.

Theoretical work was done alone with reference to journals in the fields of locomotive and automotive transportation. I developed all of the Matlab scripts and Simulink models with little help with debugging small issues.

The test rig was designed and manufactured alone with some support from the technical support staff at the university when running tests to make sure they were done safely.

The majority of problems that delayed the project were down to technical issues setting up the data logging apparatus correctly but this was resolved in the end. Furthermore, issues in the models were spotted at a late stage but were resolved before the project was finalised.

It has scope for continuation and I hope it is carried on in future years to expand on the models and create a full sized test rig.

Summary

Title: Reproducing the Vibration Environment of the SpaceX Hyperloop Test Track

Author: Daniel Carbonell

Word Count: 9853

Date: 23/04/19

This project analyses the Hyperloop test track at the SpaceX headquarters in Los Angeles, models the expected disturbances in the track, and develops an adjustable track generator to give a large sample size of possible scenarios to the track specification.

An analytical solution was derived in Matlab and a Simulink model was made for the pod with two degrees of freedom. The models allow for easy adjustments to the suspension specification of a pod and allows for the system to be optimised given a set of constraints.

A test rig was then designed and manufactured to reproduce the predicted vibration environment using an eccentric rotating mass. This test rig will be used to test components of the pod for durability and performance.

Acknowledgements

I would like to thank my project supervisor Dr Enrico Mastropaulo for taking on this project, his constructive guidance, and keeping me motivated throughout the process. His clear explanations and high standards of teaching from the dynamics course in year three sparked my interest in dynamic systems, provided a firm foundation for the content of this report and has been invaluable knowledge for the projects I have taken on since.

I also extend my thanks to the technicians and technical support staff for their help in manufacturing the test rig and performing the tests in a safe manner.

Many thanks to Arturas Jocas for his advice on modelling dynamic systems and his incredible ability to quickly find a bug in a simulation after hours if not days have been spent trying to fix the problem.

I would also like to thank my parents for their continuous support throughout the years. I am very grateful for the advice that has been given in both an academic and personal sense, they have helped me through many tough times and never lost their belief in what I can achieve when I apply myself.

Finally, I wish to express my deep gratitude for the time put into the Hyperloop project by Professor Win Rampen. His support throughout the years has been essential to the success of the team and his seemingly endless bank of knowledge has influenced countless students during the numerous design reviews he has carried out. His approach to an engineering problem of any magnitude and his ability to spot flaws in a design is truly remarkable, inspiring me to do better as an engineer and a project manager.

Notation

The following table summarises the abbreviations that are used with descriptions of what they mean.

Notation	Description
IRJ	Insulated Rail Joint
DoF	Degrees of freedom
ERM	Eccentric Rotating Mass
u	Difference in vertical height going over a step
CoM	Centre of Mass
l_1	Distance from front suspension module to CoM
l_2	Distance from rear suspension module to CoM
R_1	Reaction force on front suspension module
R_2	Reaction force on rear suspension module
J	Moment of inertia about the centre of the pod
k	Spring constant
c	Damping constant
ζ	Damping ratio
w_n	Natural frequency
w_d	Damped natural frequency
TR	Transmissibility Ratio
ESC	Electronic Speed Controller

Contents

1	Introduction	1
1.1	Abstract	1
1.2	Competition Summary	2
1.3	Aims and Objectives	2
1.4	Strategy	3
2	Literature Review	4
2.1	Modelling the Track	4
2.2	Modelling the Pod	7
2.3	Modelling the Eccentric Mass	9
2.4	Vibration Test Rigs	11
3	Track Analysis	12
3.1	Track Specification	12
3.2	Expected Step Modes	14
3.3	Track Generator	20
4	Pod Analysis	22
4.1	Vertical Suspension System	22
4.2	Weight Transfer	24
4.3	Analytical Solution	26
4.4	Numerical Solution	28
4.5	Optimisation	37
5	Test Rig	39
5.1	Concept	39
5.2	Small Scale System Design	39
5.3	Small Scale System Implementation	42
5.4	Full Scale System Concept	44
6	Results	45
6.1	First Batch	47
6.2	Second Batch	48
6.3	Possible Improvements	51
7	Conclusions	52

1 Introduction

1.1 Abstract

Accurate modelling of the expected vibration environment is critical when optimising the response of a suspension system, especially when travelling at high speed. This project analysed the Hyperloop test track at the SpaceX headquarters in Los Angeles, modelled the expected disturbances in the track, and details the development of an adjustable track generator to give a large sample size of possible scenarios. The models allow for easy adjustments to the suspension specification of a pod and allows for the system to be optimised given a set of constraints.

Inspiration for this project came from the need to simplify the design and testing process for the suspension system on the pod with a team of young and often inexperienced students. Additionally, the team is refreshed every year with many of the experienced members in their honours years leaving and their knowledge and expertise is not always passed on.

Using this model, a test rig was designed and built in order to reproduce this vibration environment to a given specification, allowing testing the performance of different pod components in a variety of different conditions. Accelerometers are attached to the moving plate to log the force created while sensors on the mounted device will collect data about vibrations transmitted to the pod through its suspension. This rig was built because it would be a valuable test for the team to verify their designs, and research has shown that such a specific device currently does not exist without paying several thousands of pounds.

Section 1. Introduction

1.2 Competition Summary

The Hyperloop is a concept envisioned by Elon Musk in 2013, where networks of tubes maintained at a low internal pressure would contain vehicles known as pods with the aim of making a new form of transportation that is faster, more energy efficient and fully electric. A competition was then started in 2015, challenging students from all around the world to build a pod and test it in the mile-long evacuated tube in Hawthorne, California next to the SpaceX headquarters - shown in Figure 1.



Figure 1: Photo of the Hyperloop test track in Hawthorne CA

1.3 Aims and Objectives

This project had six key objectives.

1. Model the track and the forces it exerts on the pod
2. Find the response of the whole system including the pod and track
3. Optimise parameters of the pod to minimise the vibrations during a run
4. Investigate a method for replicating the vibrations (i.e using an eccentric mass)
5. Build small-scale system to reproduce the vibrations
6. Scale up the small rig to accommodate the pod's suspension system

The first five targets were successfully completed and while the full scale test rig was not manufactured, a preliminary design for a potential system was made that could be passed on as a future project. Furthermore, knowing that the research, models and test rig can be used to help the team in the future is a great personal achievement.

Section 1. Introduction

1.4 Strategy

Project planning has been a crucial part of the research thus far. A regularly updated open issues list is being maintained as well as a task list for the less critical problems that need to be solved. Additionally, GitHub was used to track changes to the Matlab scripts, Simulink model and code for the microprocessor; while GrabCad was used to keep all of the 3D models backed up online.

Figure 2 shows the project plan that was executed. The project plan is split into five main sections: milestones, track, pod, manufacturing and testing. An extra three weeks was budgeted between the estimated finish date of the test rig and the report deadline for any possible contingencies. This proved to be very helpful when some unforeseen complications arose that slowed down progress.

PROJECT TITLE	Reproducing the Vibration Environment of the Hyperloop Test Track											
PROJECT MANAGER	Daniel Carbonell											
PROJECT SCHEDULE	On track											

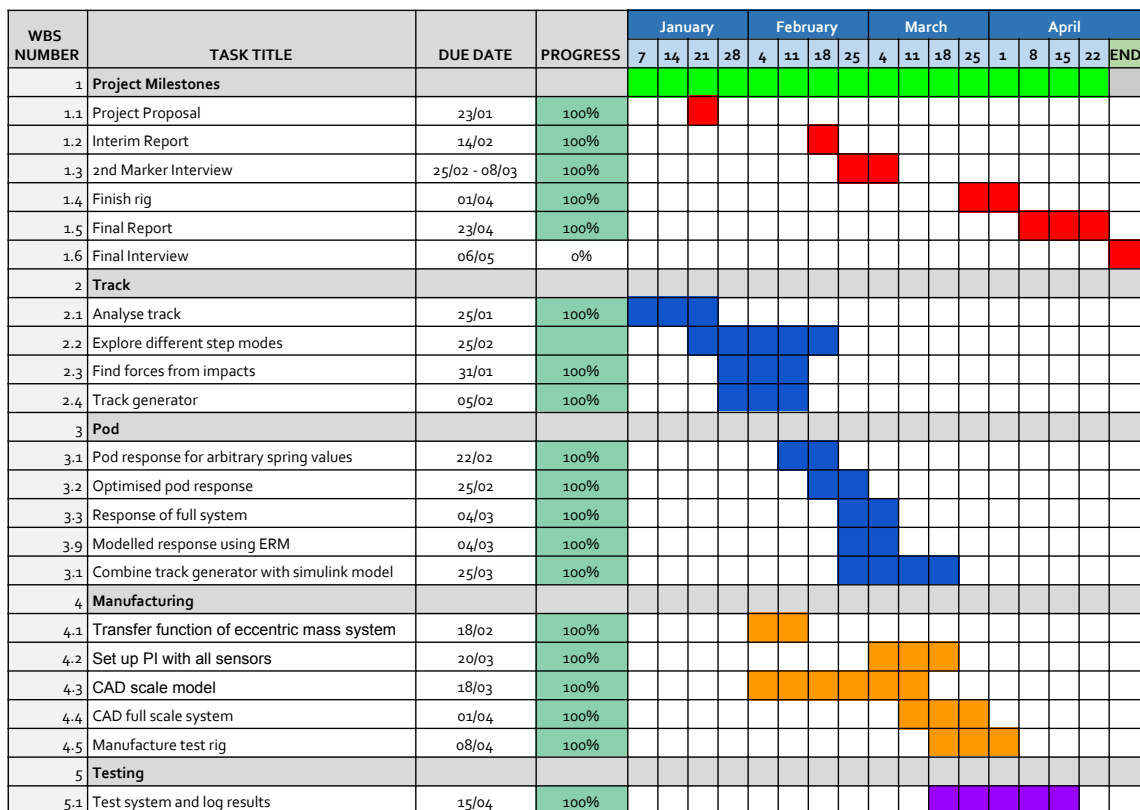


Figure 2: Gantt chart showing the executed project plan

2 Literature Review

2.1 Modelling the Track

One of the first articles to analyse the irregularities from the contact in wheel to rail systems was published in *The Railway Engineering Journal* in 1974 [1]. Their approach was to use a non-linear spring with the Hertz contact model - only accounting for dips. Figure 3 shows a representation of this model. However, this analysis was overly simplistic and does not account for discontinuities in the track causing multiple points of contact with the wheel.

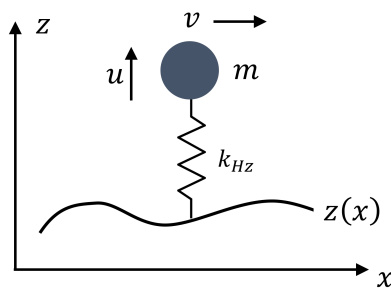


Figure 3: Free body diagram of the Hertz contact model proposed in 1974

Neglecting the possibility of a gap in the track does not include the high vertical accelerations that are a common occurrence in rail systems and a major contributor to noise during operation and damage in the track if not insulated correctly. Furthermore the Hertz contact model has since been proven false using finite element methods when insulated rail joints (IRJ) are present [2]. It was noted that the rail joints significantly changed the contact pressure and stress distributions - violating the conditions for Hertzian Theory to hold true since the contact surface was not homogeneous in these areas [3].

A better approximation was published in the *International Journal of Vehicle Mechanics and Mobility* in 2007 and uses transient double-point contact [4]. This derives the equations for the rail gaps that will be used in the model.

Single point contact occurs when there is a continuous flat rail where the wheel demonstrates rolling with no slip or instantaneous gaps on the rolling surface, it is an idealistic problem often found in textbooks covering forced vibration with Newtonian dynamics [5] [6]. Double point contact occurs whenever there is either discontinuous contact or a vertical irregularity that causes the wheel to contact multiple points on the rail. This is only applicable when the gap or step is smaller than the radius of the wheel, thus making it suitable for analysing the

Section 2. Literature Review

Hyperloop track. Figure 4 shows an exaggerated representation of both types of wheel to rail contact.

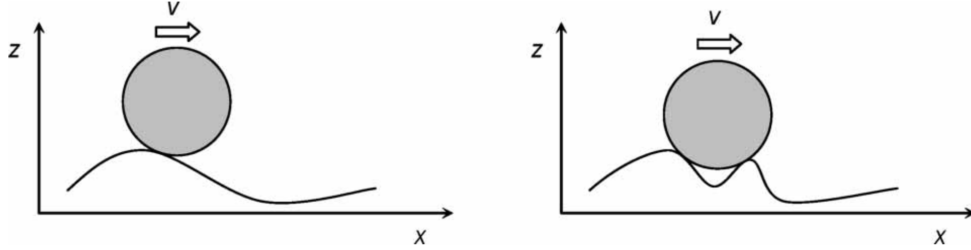


Figure 4: Single point contact is shown on the left, and double point contact is shown on the right [4]

Looking at each gap as only a vertical step simplifies the problem for initial analysis - the aim being to find the linearised trajectory of the axle of the wheel. It is also assumed that velocity is conserved when a step is encountered.

Figure 5 illustrates this trajectory where M is the mass of the wheel, R is the radius of the wheel, u_o is the height of the vertical step, v is the linear velocity of the wheel and the velocity vectors are shown with red arrows. Point A is at the instant that double point contact occurs and point B is when the wheel returns to rolling single point contact.

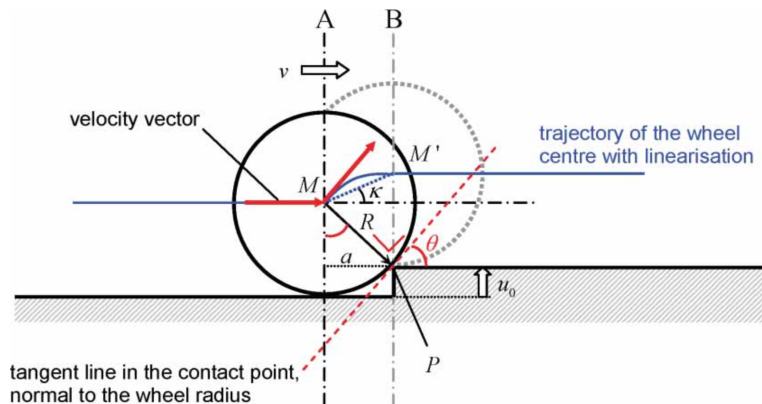


Figure 5: Wheel displacement due to a step in the track [4]

When a wheel reaches point A there is an instantaneous change in the velocity vector, changing from horizontal to tangential with the wheel at point P. This velocity can be expressed as:

$$\dot{u}(0) = v \cdot \sin(\theta) = v \cdot \sqrt{\frac{2u_o}{R}} \quad (1)$$

Section 2. Literature Review

The chord of the circle shown as a in the schematic is required to find the function for vertical displacement with respect to time.

$$a = \sqrt{u_o(2R - u_o)} \approx \sqrt{2Ru_o} \quad \text{when} \quad u_o \ll R \quad (2)$$

Again, with $t = 0$, $x = 0$ occurring at position A, and $0 < x < a$:

$$z(t) = \frac{u_o}{a} \cdot x = \sqrt{\frac{u_o}{2R}} \cdot x = \sqrt{\frac{u_o}{2R}} \cdot v \cdot t_a \quad (3)$$

By graphically representing the wheel trajectory, shown in Figure 6 displacement can now be written in continuous time by using the Heaviside-function H :

$$z(t) = \frac{u_o \cdot t}{t_b} \cdot H(t_b - t) + u_o \cdot H(t - t_b) \quad (4)$$

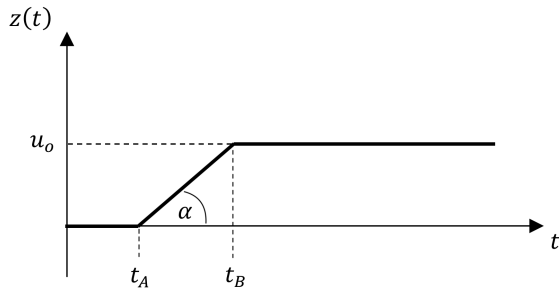


Figure 6: Linear trajectory of wheel axle in time domain after rolling over a step

Where t_a is the point in time when the wheel impacts the step, t_b is the point in time after rising over the step has been and t_b is given by the distance travelled over the current linear speed:

$$t_b = \frac{\sqrt{2Ru_o}}{v} \quad (5)$$

Finally, combining the above equation results in the vertical displacement function in terms of speed, time and the parameters of both the wheel and step:

$$z(t) = \sqrt{\frac{u_o}{2R}} \cdot v t \cdot H\left(\frac{\sqrt{2Ru_o}}{v} - t\right) + u_o \cdot H\left(t - \frac{\sqrt{2Ru_o}}{v}\right) \quad (t \geq 0) \quad (6)$$

2.2 Modelling the Pod

Similarly to modelling a car with six degrees of freedom, the response to external stimuli can be derived using either the Newton-Euler approach [7] [8] or with Lagrange's equations [9]. The equations of motion will contain three linear vectors: vertical (z), longitudinal (x) and lateral (y); along with three angular vectors: pitch, roll and yaw. Figure 7 shows these degrees of freedom with respect to the motion of the pod along the track.

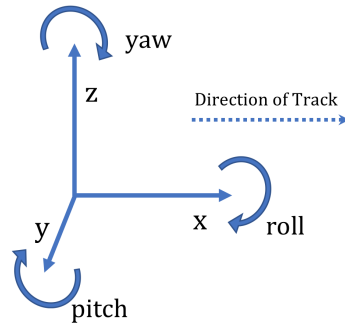


Figure 7: Degrees of freedom about the centre of mass

While this approach provides the most accurate model, it can initially be simplified to an approximate two degree of freedom system with the assumption that the track is perfectly straight in the lateral axis, and that roll will be comparatively small and therefore negligible. Additionally, since the suspension module uses a rocker system with a 1:1 ratio it can be simplified to a spring contacting the track surface.

Suitable values for spring and damping constants can be found only for changes in z height and pitch following another article on analysing car suspension [10]. Here Lagrange's equations (7) are solved for each degree of freedom to model a car travelling over rough terrain assuming that roll is negligible compared to bounce (z direction) and pitch - shown in Figure 8.

$$\frac{d}{dt} \left(\frac{\partial T}{\partial \dot{q}_i} \right) - \frac{\partial T}{\partial q_i} + \frac{\partial V}{\partial q_i} = Q_i \quad (7)$$

Where T is kinetic energy, V is potential energy, Q is energy loss in the system and q_i represents a degree of freedom.

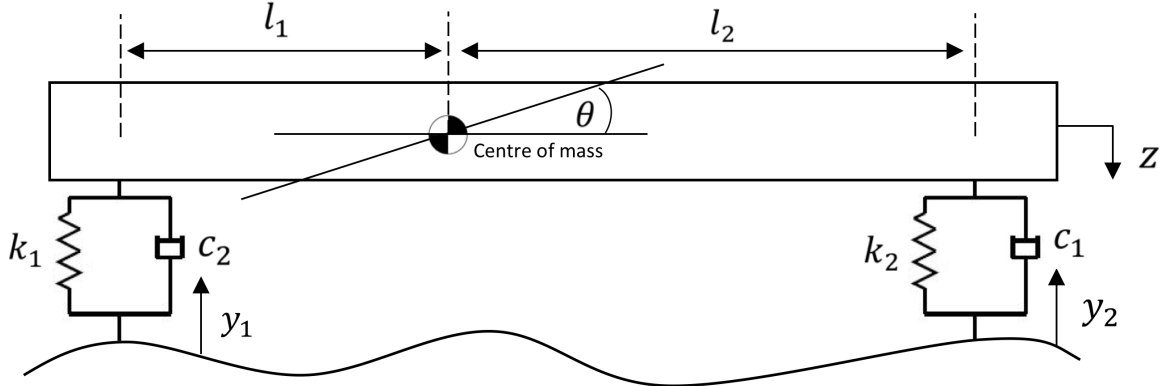


Figure 8: Simplified two degree of freedom free body diagram

By analysing the system, kinetic and potential energy functions are obtained respectively as follows:

$$T = \frac{1}{2}m\dot{z}^2 + \frac{1}{2}J\dot{\theta}^2 \quad (8)$$

$$U = \frac{1}{2}k_1(y_1 - z + l_1\theta)^2 + \frac{1}{2}k_2(y_2 - z - l_2\theta)^2 \quad (9)$$

With the energy dissipated in the damper expressed as:

$$Q = \frac{1}{2}c_1(\dot{y}_1 - \dot{z} + l_1\dot{\theta})^2 + \frac{1}{2}c_2(\dot{y}_2 - \dot{z} - l_2\dot{\theta})^2 \quad (10)$$

With the highly constrained space inside of the pod, the stiff spring required to support the weight of the pod, energy losses due to elastic deformation in the spring - known as the material's damping capacity - was thought to provide the desired damping.

This property has been found experimentally for many different materials [11]. Taking steel alloys as the most commonly used material in springs [12], different steel alloys have a damping ratio of around 0.15×10^{-3} to 3×10^{-3} - while viscous dampers in cars typically have a damping ratio of around 0.3 [13].

Using this data it is highly unlikely that the damping capacity alone will be sufficient to effectively attenuate the vibrations of the pod during operation.

2.3 Modelling the Eccentric Mass

This part of the model will be relatively simple to generate following the procedure of modelling an unbalanced mass described in detail in the *Mechanical Vibrations* textbook cited earlier [5]. In this part of the system there is an eccentric rotating mass (ERM) revolving within a structure that is free to move in the vertical direction but constrained laterally - shown in Figure 9. As the motor rotates at a given angular velocity, the imbalance causes the centre of mass of the entire system to oscillate in a circular motion. However, since the walls of the system are constraining its movement, it can only move vertically. Thereby the rail on which the pod is mount will be attached to the upper surface shown on the schematic.

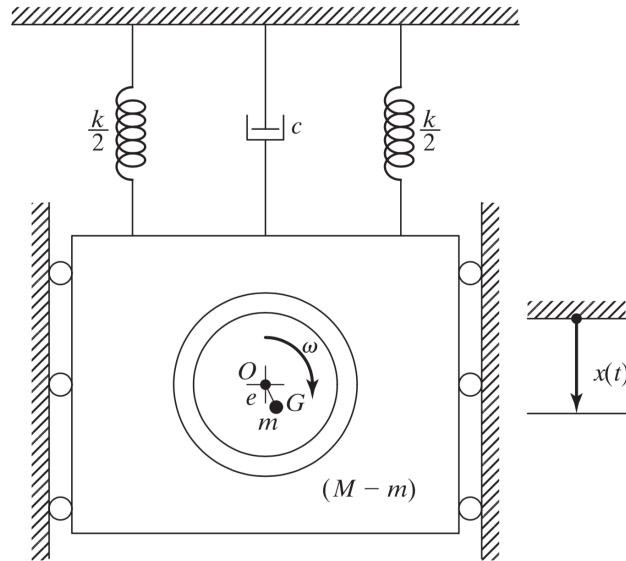


Figure 9: Schematic of a system containing a rotating imbalance [5]

The equation of motion of this system is as follows:

$$M\ddot{x} + c\dot{x} + kx = F_0 \sin(\omega t) \equiv m\omega^2 \sin(\omega t) \quad (11)$$

Where M is the total mass of the system, m is the mass of the rotor, ω is the angular velocity of the mass, and e is the distance from the principal axis of rotation. The force transmissibility ratio to the base (top of schematic) is then expressed as:

$$T_f = \frac{F_t}{m\omega^2} = \frac{F_t}{mer^2\omega_n^2} \quad (12)$$

Where F_t is the transmitted force, ω_n is the natural frequency of the spring and r is the frequency ratio ($r = \frac{\omega}{\omega_n}$).

Section 2. Literature Review

Using the equation for transmissibility ratio, equation (12) can be rearranged to find the transmitted force.

$$F_t = m\omega^2 \left(\frac{1 + (2\zeta r)^2}{(1 - r^2)^2 + (2\zeta r)^2} \right)^{\frac{1}{2}} \quad (13)$$

Where ζ is the damping ratio of the system in the vertical direction.

An anticipated challenge will be to accurately match the forced frequency and transmitted force to a given rotational speed and torque in the motor. Especially since the high linear acceleration of the pod (approximately $7m/s^2$) means that both the frequency of oscillation and the change in vertical forces due to bumps in the track with respect to time will be high. For these reasons alternative methods have been explored when researching the field.

2.4 Vibration Test Rigs

The optimal method of excitation would be analogous to how synthetic suspension tests are carried out by car manufacturers - by using a hydraulic system [14] [15]. In both of referenced articles, a quarter-car test rig is built to mount the suspension and wheel system which is then excited by a linear hydraulic actuator which vibrates a platform. Figure 10 shows the test rig used in article [15].



Figure 10: Quarter car test rig used in *American Control Conference, 2004* [15]

These are sold commercially and can easily supply several kilo-Newtons of dynamic force at several hundreds of hertz [16].

Unfortunately the cost to purchase a hydraulic reservoir, pump, control and relief valves, as well as double acting cylinder would far surpass the budget of this project. Nevertheless, reference can still be made to the aforementioned articles with regards to the control system used in the test rigs.

There are already four 75kW motors in the Hyperloop team's possession which is the main reason for pursuing the method using an ERM.

Section 3. Track Analysis

3 Track Analysis

3.1 Track Specification

The track is a 1.2km air-tight steel tube capable of maintaining a partial vacuum at 860Pa. Within this tube there are tube utilities fixed to the top of its inside, and a concrete foundation on the base. There are two important features rigidly attached to this concrete base: an aluminium sub-track and an aluminium I-beam. Both of these provide teams with flexibility in their designs, encouraging different methods to clamp the monorail as well as providing a conductive surface to facilitate magnetic levitation systems.

Since the vertical suspension system will rest on the flange of the I-beam, this will be the part of the tube under investigation. It is made of discrete I-beam sections bolted to the base of the tube, therefore the many discontinuities introduced by the gaps between sections are perceived as steps during a run. Since these gaps have a height and width in a known range, their impact on the stability of the pod can be modelled in accordance with the pod's trajectory to the upper and lower limits given by the track specification [17].

The following technical drawing shown in Figure 11 (taken from the competition rules and regulations) shows a cross sectional view of the tube including dimensions and tolerances of both the I-beam and sub-track. All measurements are in inches.

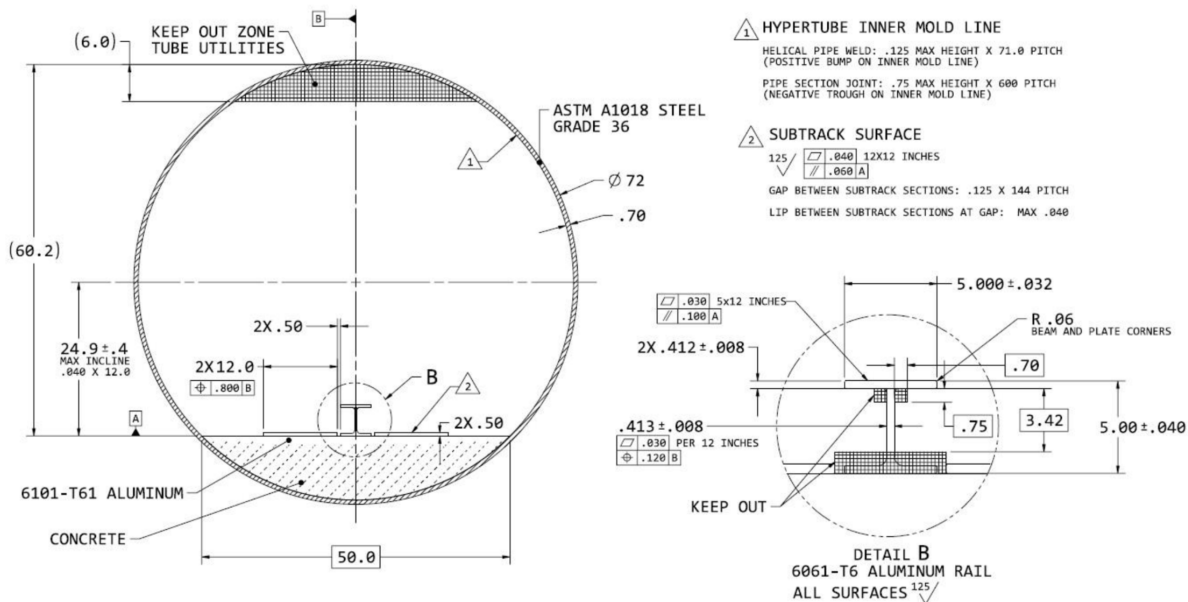


Figure 11: Technical Drawing of Hyperloop Test Track (including aluminium central rail) [17]

Section 3. Track Analysis

While the figure includes all of the dimensions, the most relevant details of the track are summarised in Table 1. The highly specific tolerances arose due to the conversion from imperial to SI units. It is also mentioned that there may or may not be a non-conductive insulator between rail joints.

Table 1: SpaceX Hyperloop track summary

Track Feature	Specification
Material	Aluminium 6061-T6
Distance between rail gaps	3.81m
Gap size	2.54mm - 3.175mm
Max. step in height	Under 1.016mm
Flatness Profile (381x381mm)	1.016mm
Instantaneous bends	0.16°(Pitch) 0.07°(Yaw)
Max. variation of top plane	10.16mm
Max. longitudinal slope	1.061mm per 304.8mm
Max. lateral slope	1.52mm per 3810mm

The focus of this investigation will be on a two degree of freedom model of the pod finding pitch and bounce. Therefore, the gap size, step in height and distance between gaps are the most significant contributors to the excitation of the suspension system.

3.2 Expected Step Modes

There are three expected modes of contact with a joint in the track. These are an even gap (a), a step up (b), and a step down (c) - illustrated in Figure 12. As can be seen, each will feature a gap in the rail, but only the latter two show a change in vertical displacement.

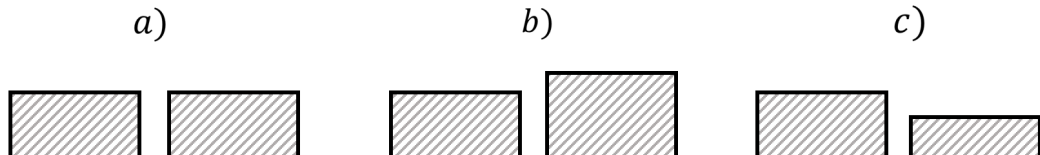


Figure 12: Three main modes of contact at rail joints

Each discontinuity is analysed as a ramp with a change in vertical displacement with respect to time, allowing for the rise time, speed and force caused by a bump after each impact to be determined. Given that the size of the steps and gaps are very small with regards to the radius of the wheels, each trajectory is approximated to be linear to simplify the problem. It is also assumed that velocity is conserved when the wheel travels over a step.

3.2.1 Vertical Step

In this mode, there is a sudden change in the height of the track causing a rapid change in the trajectory of the wheel. Figure 13 illustrates this trajectory r is the radius of the wheel u is the height of the vertical step, v is the linear velocity of the wheel and the velocity vectors are shown with red arrows.

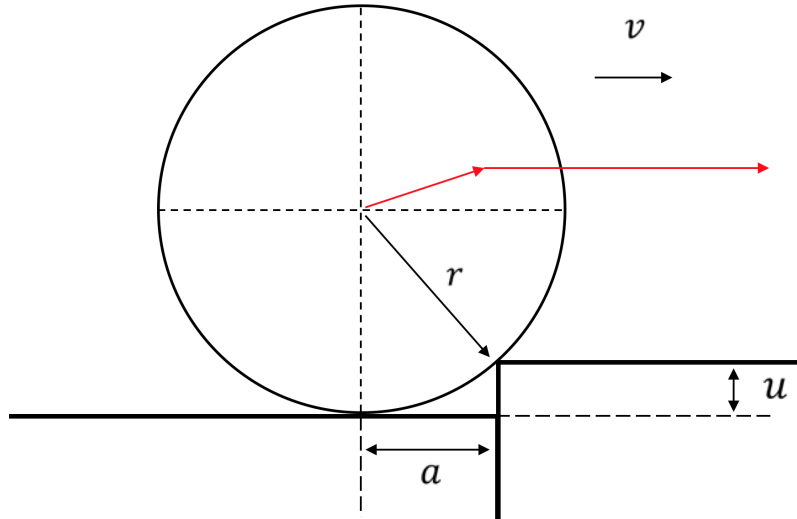


Figure 13: Wheel displacement due to step in track

All that is required to model this mode is the change in height u and the time taken to reach that height, then the points in between can be interpolated. The distance a can be found using Pythagoras theorem:

$$a = \sqrt{u(2r - u)} \quad (14)$$

Where r is the radius of the wheel and u is the step height. Then the rise time can be found by dividing this distance by the current speed of the pod.

$$t = \frac{\sqrt{u(2r - u)}}{v} \quad (15)$$

This is a simplified representation to how it was done previously and relies on the fast interpolation functions built into Matlab to model the track to complete the same operation with less CPU time.

3.2.2 Even Gap

In this mode there is no change in height but there is a gap between the two sections of track. This will cause a symmetrical drop and rise as the gap is covered. Figure 14 shows the geometry of a wheel in an even gap, with the expected trajectory of the centre of the wheel shown in red. This is a highly unlikely scenario but it will be analysed nonetheless.

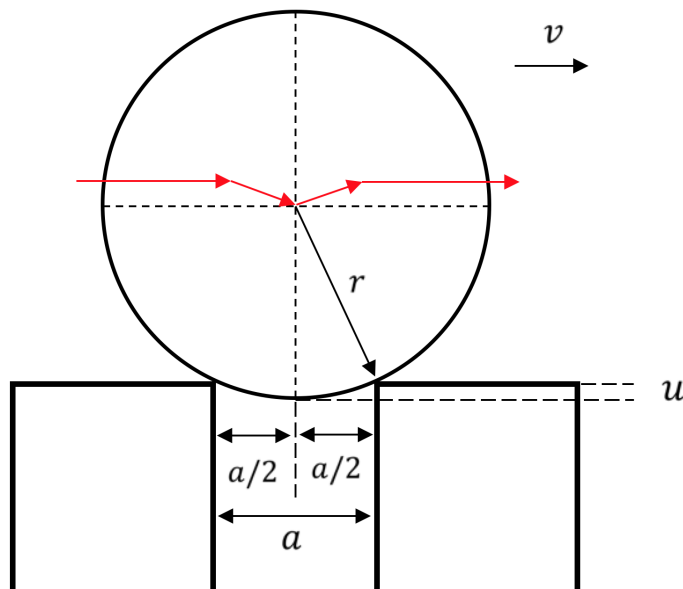


Figure 14: Wheel displacement due to gap in track

This is a very similar problem to analyse as the step problem, however in this case, the chord of the circle is of a known length while the vertical change in height is not. The radius can be calculated as follows.

$$r^2 = (a/2)^2 + (r - u)^2 \quad (16)$$

Where a is the separation of the track sections, this equation can be rearranged to:

$$a = \sqrt{4u(u - 2r)} \quad (17)$$

With the rise time being the distance travelled divided by the current speed.

$$t_r = \frac{a/2}{v} \quad (18)$$

This is the required equation to model the gap but the value of u is still unknown. Rearranging for u gives the following expression:

Section 3. Track Analysis

$$u = r \pm \frac{\sqrt{-(a-2r)(a+2r)}}{2} \quad (19)$$

Given a gap size of $a = 3\text{mm}$ and a wheel radius of $r = 40\text{mm}$, substituting these values into equation 19 shows that:

$$u = 2.813489 \times 10^{-5}\text{m} \quad \text{and} \quad u = 7.997187 \times 10^{-2}\text{m}$$

The latter is far too large and is much closer to the diameter of the wheel than the gap size. The accuracy of these equations were validated using a CAD package (Solidworks), (see Figure 15).

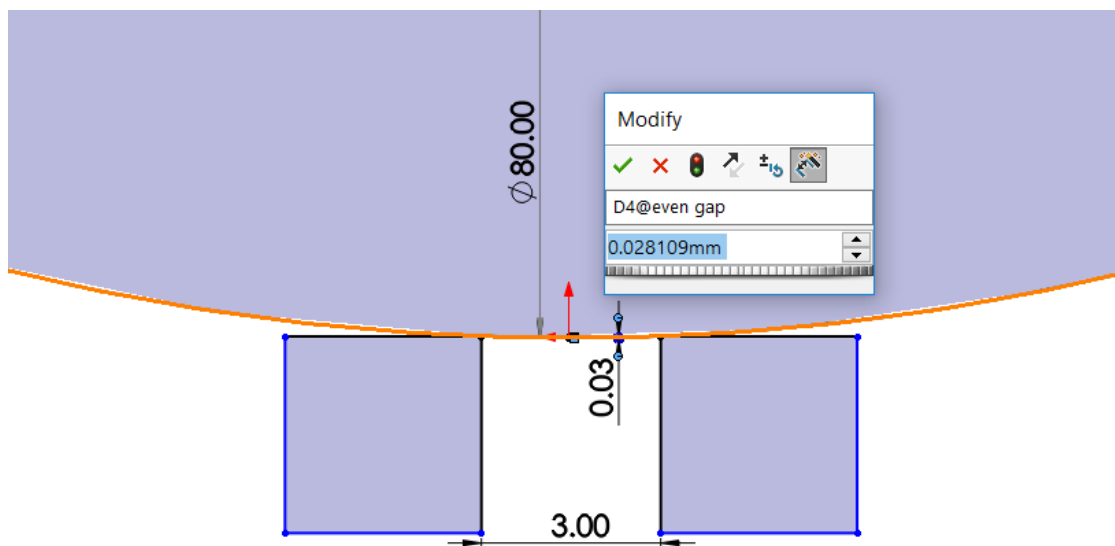


Figure 15: Validation of gap equation using CAD package

With a value of $2.8109 \times 10^{-5}\text{m}$, this proves the equations are only valid for the first solution with a difference of only 0.092%. Therefore, the appropriate form of this equation is:

$$u = r + \frac{\sqrt{-(a-2r)(a+2r)}}{2} \quad (20)$$

However, this step mode has very little effect on the suspension system with a vertical change in height of under 0.03mm at the maximum specified gap size. Given that this is very small compared to the vertical step, it will not be considered as the common case when optimising the response of the pod.

3.2.3 Vertical Step with Gap

The last mode of contact to discuss combines the previous two into a problem with a step and a gap. With a small enough wheel radius, this should cause an asymmetrical fall and rise at the centre of mass of the wheel. Figure 16 illustrates this mode of contact.

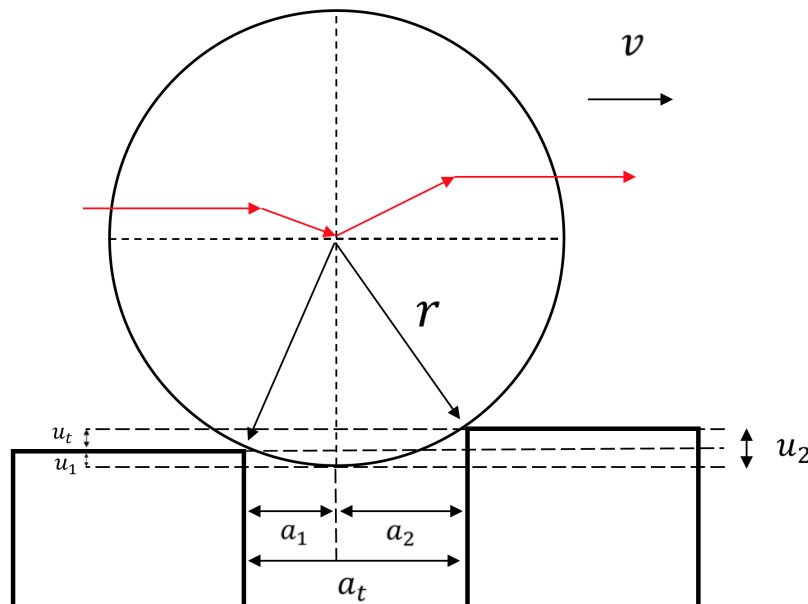


Figure 16: Schematic of double point contact with a gap step

This problem is slightly more complicated than the previous two as there are more variables in the equations and the majority are undefined. Before deriving the equations, Table 2 below summarises the variables in question.

Table 2: Known and unknown variables in the uneven gap scenario

Definition	Symbol	State
Step up	u_t	known
Step down	u_1	unknown
total Vertical distance	u_2	unknown
Gap size	a_t	known
first gap	a_1	unknown
second gap	a_2	unknown
Velocity	v	known
wheel radius	r	known

All of the unknown parameters can be solved using the known values in four equations to fully define the trajectory of a wheel in this mode, each equation has two unknown values.

Section 3. Track Analysis

The four equations are as follows:

$$r^2 = a_1^2 + (r - u_1)^2 \rightarrow a_1 = \sqrt{u_1(2r - u_1)} \quad (21)$$

$$r^2 = a_2^2 + (r - u_2)^2 \rightarrow a_2 = \sqrt{u_2(2r - u_2)} \quad (22)$$

$$u_2 = u_t + u_1 \quad (23)$$

$$a_t = a_1 + a_2 \quad (24)$$

Combining 21 and 23 leads to an expression for the distance of the first section of the wheel trajectory.

$$a_1 = \sqrt{(u_2 - u_t)(2r - u_2 + u_t)} \quad (25)$$

Which can finally be combined with equation 24 to give an expression for the total gap (a_t) with only one unknown (u_2):

$$a_t = \sqrt{(u_2 - u_t)(2r - u_2 + u_t)} + \sqrt{u_t(2r - u_2)} \quad (26)$$

This can be rearranged to find the value of u_2 :

$$u_2 = r + \frac{u_t}{2} \pm \frac{a_t \sqrt{\frac{-a_t - 4r^2 + u_t^2}{a_t^2 + u_t^2}}}{2} \quad (27)$$

When this mode was checked in CAD it was found that there is no dip in the wheel trajectory since the wheel is much larger than the gap and there would only be a dip if the radius of the wheel is less than the value of a_t .

Applying the dimensions of the pod wheel and a 1mm step, it was found that the minimum gap size required for the wheel to dip before double point contact is 8.89mm, which is 2.8 times larger than the maximum specified gap size.

Section 3. Track Analysis

3.3 Track Generator

In order to simulate the dynamic response of the pod during operation, a track generator was developed in Matlab. This links with the trajectory script used to calculate the pod speed during a test run and takes samples at 3.8m intervals - the locations of the rail discontinuities.

Taking this sampled speed, the equations derived in section 3.2.1 can be applied with a known step height to find the rise time of the wheel; from the point of impact to the point where the wheel is at a tangent to the new section of rail. The height of each step is randomly generated within a range of given values and the direction of the step is randomly alternated in the positive and negative direction. The random elements are implemented to account for the uncertainty in the track, allowing for many iterations of the vibration script to optimise for a larger sample size. Figure 17 shows a flow chart of the track generator in operation.

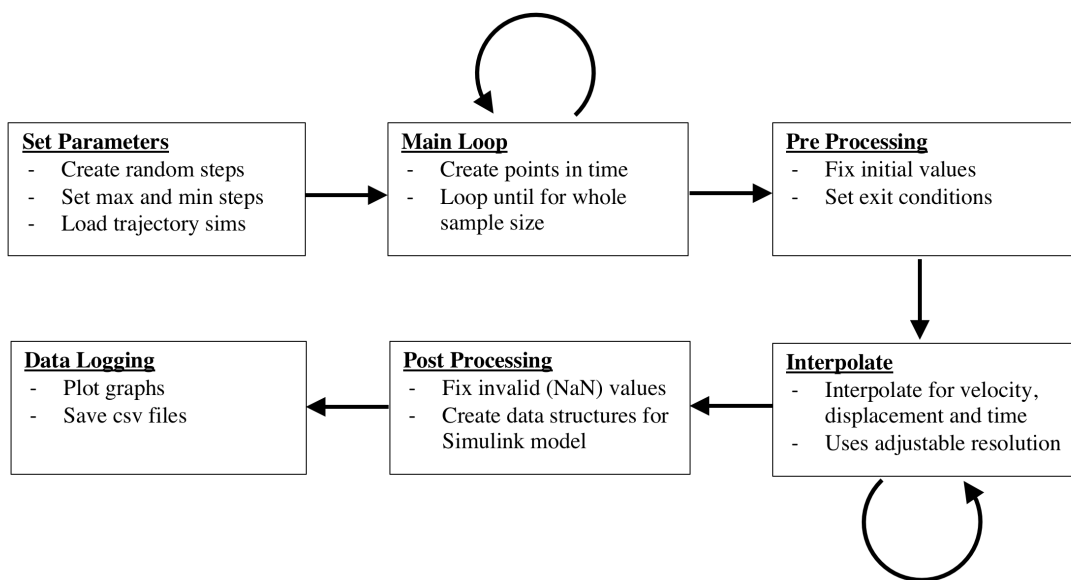


Figure 17: Flow chart of the track generator

Now that there are recorded points containing the change in vertical displacement in time at impact and after rising, these unconstrained values are put through an interpolating function which rapidly generates a set of coordinates to a specified resolution. An output from the generator with a step size in the range of 0.5mm-1.1mm is shown below in Figure 18.

Section 3. Track Analysis

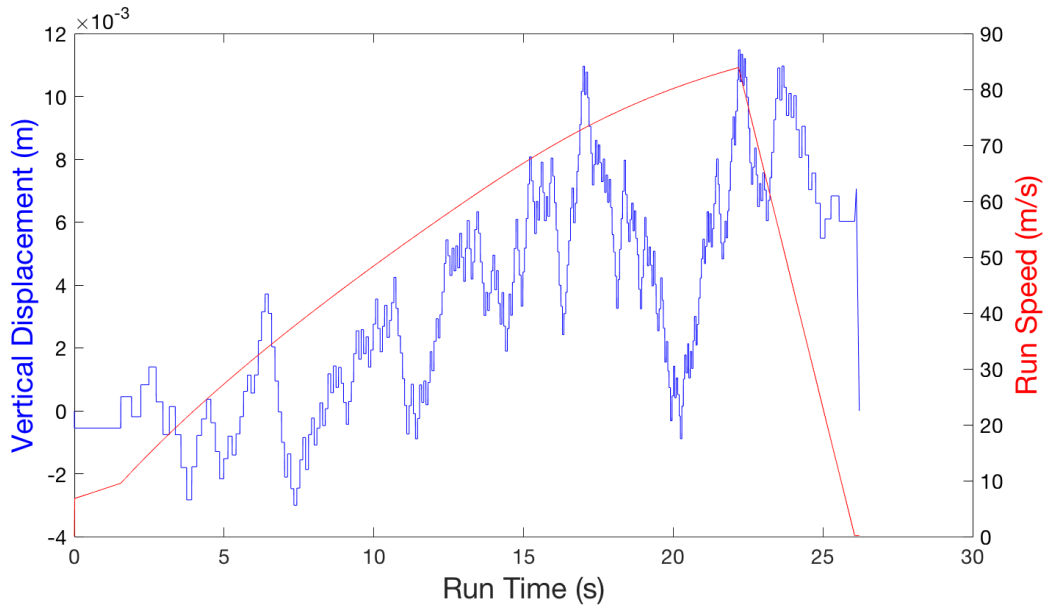


Figure 18: Output from track generator script

The blue line represents the vertical displacement while the red line represents the current pod speed at the given time. As expected, the frequency of disturbances (shown by the width of the plateau of each step) increases with the pod speed and conversely, decreases as the pod slows to a stop.

It appears that the track generator creates vertical steps, but zooming in on the plot reveals that it is in fact made of many ramps of varying gradients. The rise time in every model based on the current trajectory simulations with an acceleration of $0.7g$ and deceleration of $2.2g$ shows a minimum rise time of 81.35 microseconds at top speed and a maximum of 54.5 milliseconds right as the pod begins to accelerate. These two points are shown in Figure 19 a and b.

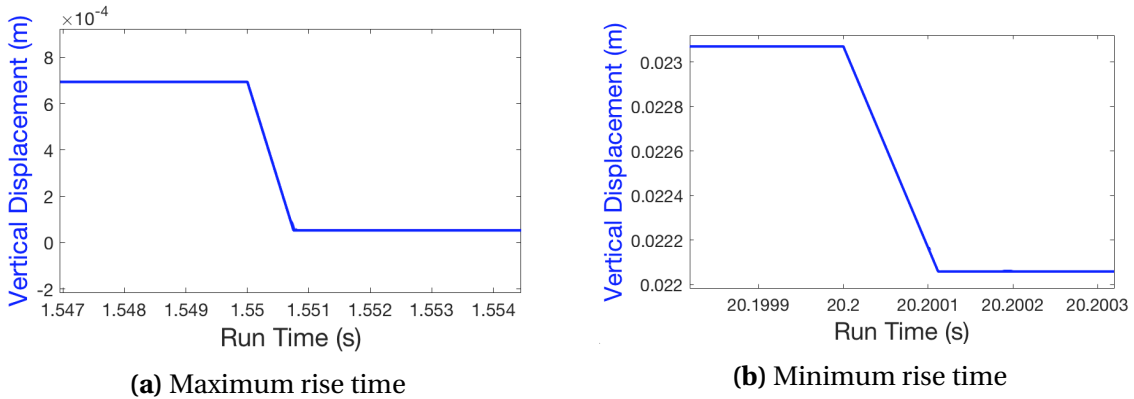


Figure 19: Maximum and minimum rise time of wheel over a step in the track

4 Pod Analysis

4.1 Vertical Suspension System

The overall function of the rocker and wheel system is to make sure the pod rides smoothly along the I-Beam and is kept vertically stable despite irregularities in the track. After using a mountain bike shock absorber for last year's suspension, it was noted that the chosen model was too stiff, and did not provide the appropriate form of stabilisation for the high speed, low deflection conditions that would occur in a Hyperloop run.

Subsequently, a spring and rocker system was adapted to better cope with the irregularities at high speed, shown in Figure 20. Small wheels (60mm in diameter) are used to save space within the chassis and to keep the pod as close as possible to the I-Beam, contributing to better aerodynamics and a lower centre of mass. The material for the wheel is nylon for its strength, durability and abrasion resistance. Furthermore, the material was tested extensively last year for the stability subsystem and proved to be ideal.

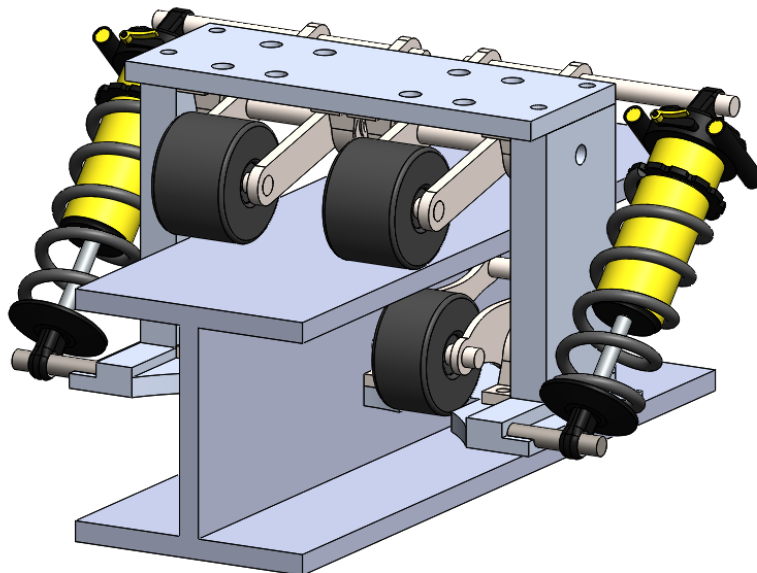


Figure 20: 3D model of the suspension system to be used on the pod

The rocker itself is made from stainless steel 314 chosen for its strength despite its high density - given that the rocker structure is small. The surrounding structure, which is much larger, was chosen to be made from aluminium to save mass. The overall dimensions of the subsystem are 150 x 170 x 260 mm and the total mass is 24 kg.

Section 4. Pod Analysis

On the outer sides of the module there is a coil-over shock absorber acting as the main spring and dampers on the pod. They are mounted to the same point where the wheel attaches to the rocker and are supported at the base of the module. This design was chosen since it provides the largest distance for a shock absorber to fit inside the pod, allowing for more flexibility with the component selection.

Along the bottom section of the module are two more tension springs used to restrict the pods movement in the positive vertical direction to prevent any other components from hitting the I-beam and stop the pod from derailing in the event of a critical failure.

4.2 Weight Transfer

Whenever a vehicle accelerates, moments from forces at the supports and the centre of mass cause the load taken by each of its wheels to be unevenly distributed. For example in a car, more of the weight transfers to the back wheels when accelerating, causing it to pitch; and for the same reason the centripetal force generated when taking a sharp corner causes the car to roll.

It is only expected that the pod will pitch since there are no bends in the track, the free body diagram for this problem is shown in Figure 21 where the wheels are represented as rigid contact points.

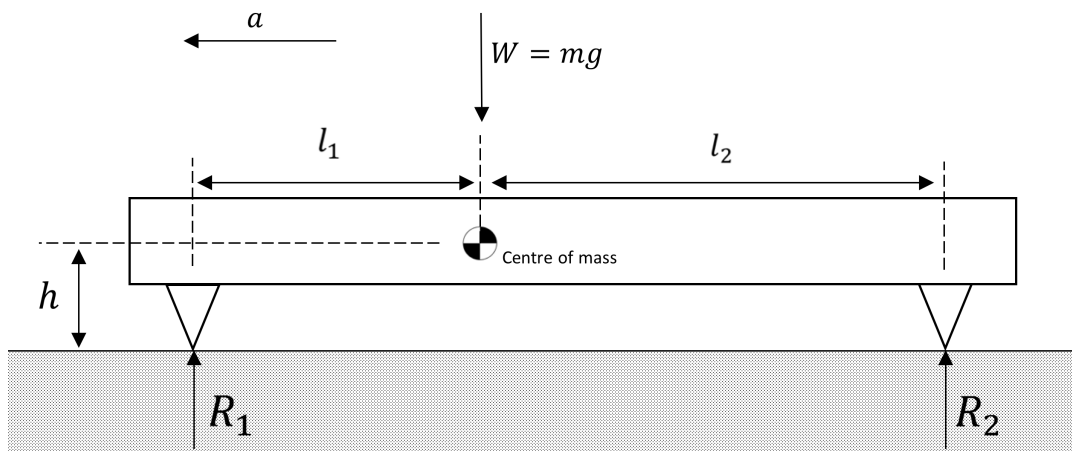


Figure 21: Side view free body diagram of vehicle accelerating

Taking moments about each support gives:

$$\sum M_{R1} = 0 = (l_1 + l_2)R_2 + mgL_1 - mah \quad (28)$$

$$\sum M_{R2} = 0 = -(l_1 + l_2)R_1 + mgL_2 + mah \quad (29)$$

Where M is the moment about the contact point, a is the current acceleration, h is the distance from the top of the I-beam to the CoM, l_1 and l_2 are the distances from the centre of mass to the front and rear wheels, R_1 and R_2 are the forces on the front and rear wheels respectively. The distances to the supports are $l_1 = 620\text{mm}$, $l_2 = 630\text{mm}$ and the distance from the rail to centre of mass is $h = 30\text{mm}$. This Low h value comes from the design philosophy to lower the CoM and reduce the total weight transfer.

Section 4. Pod Analysis

These equations can be rearranged to find the reaction forces on each support:

$$R_1 = \frac{mgl_2 - mah}{l_1 + l_2} \quad (30)$$

$$R_2 = \frac{mgl_2 + mah}{l_1 + l_2} \quad (31)$$

Bearing in mind that the total weight of the pod is the sum of these reaction forces.

$$W = mg = R_1 + R_2 \quad (32)$$

Finally, the ratio of load on the front wheel is as follows:

$$\text{Load Ratio}_{front} = \frac{R_1}{W} \quad \text{Load Ratio}_{rear} = \frac{R_2}{W} \quad (33)$$

A Matlab script linked with the pod trajectory was made to find the load ratio on the front wheel. This was then passed to the Simulink model as one of the most critical components.

The current speed and ratio of load on the front wheel in time is shown in Figure 22.

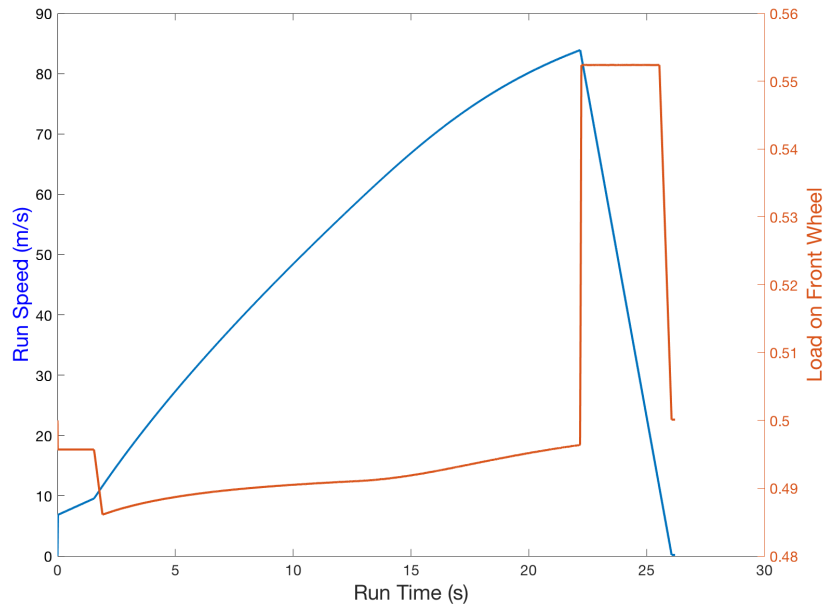


Figure 22: Load ratio on front wheel aligned with current pod speed

By inspection, these values seem reasonable since the load is expected to be lower during the acceleration stage and then spike up when the brakes are applied.

4.3 Analytical Solution

Expanding on the equations formed using the free body diagram in section 2.2 - shown in Figure 23 - gives the equations of motion for the two DoF system:

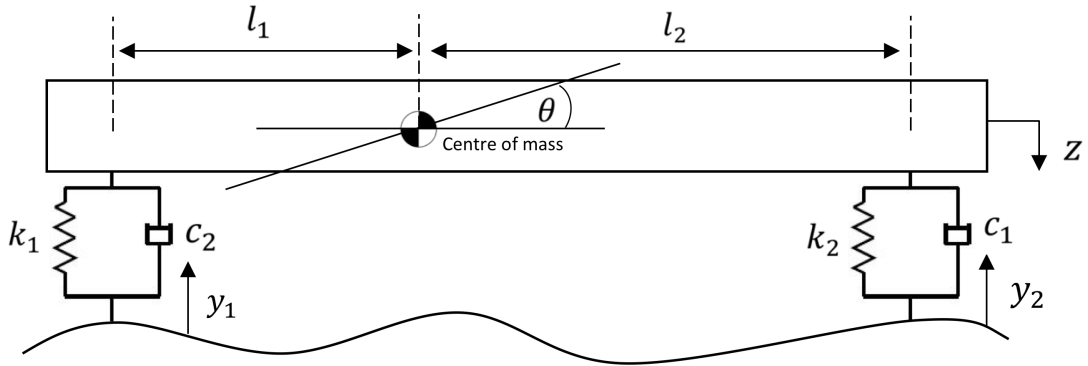


Figure 23: Free body diagram of the two degree of freedom system

$$\begin{aligned} m\ddot{z} + (c_1 + c_2)\dot{z} + (l_2 c_2 - l_1 c_1)\dot{\theta} + (k_1 + k_2)z + (l_2 k_2 - l_1 k_1)\theta \\ = k_1 y_1 + k_2 y_2 + c_1 \dot{y}_1 + c_2 \dot{y}_2 \end{aligned} \quad (34)$$

$$\begin{aligned} J\ddot{\theta} + (c_2 l_2 - c_1 l_1)\dot{z} + (l_2^2 c_2 + l_1^2 c_1)\dot{\theta} + (k_2 l_2 - k_1 l_1)z + (l_1^2 k_1 + l_2^2 k_2)\theta \\ = k_2 l_2 y_2 - k_1 l_1 y_1 + k_1 l_1 \dot{y}_2 + c_2 l_2 \dot{y}_1 \end{aligned} \quad (35)$$

Matlab is used to solve these differential equations due to their complexity. First the equations of motion are changed into matrix form:

$$\begin{aligned} \begin{bmatrix} m & 0 \\ 0 & J \end{bmatrix} \begin{bmatrix} \ddot{x} \\ \ddot{\theta} \end{bmatrix} + \begin{bmatrix} c_1 + c_2 & l_2 c_2 - l_1 c_1 \\ l_2 c_2 - l_1 c_1 & l_2 c_2 + l_1^2 c_1 \end{bmatrix} \begin{bmatrix} \dot{y}_1 \\ \dot{\theta} \end{bmatrix} + \begin{bmatrix} k_1 + k_2 & k_2 l_2 - k_1 l_1 \\ k_2 l_2 - k_1 l_1 & l_1^2 k_1 + l_2^2 k_2 \end{bmatrix} \begin{bmatrix} x \\ \theta \end{bmatrix} \\ = \begin{bmatrix} k_1 & k_2 \\ -k_1 l_1 & k_2 l_2 \end{bmatrix} \begin{bmatrix} y_1 \\ y_2 \end{bmatrix} + \begin{bmatrix} c_1 & c_2 \\ -c_1 l_1 & c_2 l_2 \end{bmatrix} \begin{bmatrix} \dot{y}_1 \\ \dot{y}_2 \end{bmatrix} \end{aligned} \quad (36)$$

To find the damped harmonic response, the right hand side of the equation is set to zero and the non-trivial solutions to the equations can be evaluated by finding the determinant of the characteristic equation:

$$\det \begin{bmatrix} ms^2 + (c_1 + c_2)s + k_1 + k_2 & (l_2 c_2 - l_1 c_1)s + k_2 l_2 - k_1 l_1 \\ (l_2 c_2 - l_1 c_1)s + k_2 l_2 - k_1 l_1 & Js^2 + (l_2^2 + l_1^2 c_1)s + (l_1^2 k_1 + l_2^2 k_2) \end{bmatrix} \quad (37)$$

Section 4. Pod Analysis

The *conv()* function is now used here to convolve the diagonal elements of the matrix before they are subtracted. Now the *roots()* function is used to find the roots of the equation with any values of k or c. A spring rate of 50,000 and a damping constant of 100 gives the following roots:

$$s = \begin{bmatrix} -0.3518 + j19.1484 \\ -0.3518 - j19.1484 \\ -0.3212 + j17.4969 \\ -0.3212 - j17.4969 \end{bmatrix} \quad (38)$$

Where the absolute imaginary value of each complex conjugate pair are the first and second damped natural frequencies, and the negative sign in the real parts of the equation is the product of the damping ratio and natural frequency, showing the decaying nature of this system. The following equations are now formed:

$$\omega_d = \omega_n \sqrt{1 - \zeta^2} \quad \rightarrow \quad \omega_d = \sqrt{\omega_n^2 - (\omega_n \zeta)^2} \quad (39)$$

Where ω_n is the natural frequency, ω_d is the damped natural frequency, and ζ is the damping ratio of the system. Equation 39 can be rearranged to find the natural frequency:

$$\omega_n = \sqrt{\omega_d^2 + (\omega_n \zeta)^2} \quad (40)$$

The values in the square root are can be found from s, where $-\zeta \omega_n = \text{Re}(s)$ and $\omega_d = \text{Im}(s)$. Using the same values of k and c, the two damped and undamped natural frequencies are:

$$\omega_{d1} = 19.1484 \quad \omega_{d2} = 17.4969$$

$$\omega_{n1} = 19.1516 \quad \omega_{n2} = 17.4999$$

Giving a damping ratio for the first and second frequencies of $\zeta_1 = 0.01837$ and $\zeta_2 = 0.01835$ respectively.

4.4 Numerical Solution

A Simulink model of the pod was made in order to combine all of the previously mentioned analysis allowing for visualisation and optimisation of the suspension system parameters. The model is split into time steps which are imported from the output of the track generator mentioned in section 3.3, allowing the generated track disturbances to stimulate the suspension system.

This model is split into five main sections:

- Weight shift - to find how the load is distributed to the wheels
- Front wheel - to find displacement and forces on the front pair of wheels
- Rear wheel - to find displacement and forces on the rear pair of wheels
- Moment - to find the angular pitch of the pod
- Bounce - to find the vertical movement of the pod

In each loop, a force is found which is then divided by a known mass to give acceleration. This can then be integrated either once or twice to find velocity or displacement respectively. These values can then be used to find a new force and the loop continues. The following sections will describe each subsystem in more detail.

4.4.1 Weight Shift

The blocks shown in Figure 24 take the weight transfer at every time step based on the acceleration of the pod that was calculated by the track generator. These values are then used to calculate the distributed weight on the front and rear wheels and is passed to a go-to block so it can be used in other parts of the model.

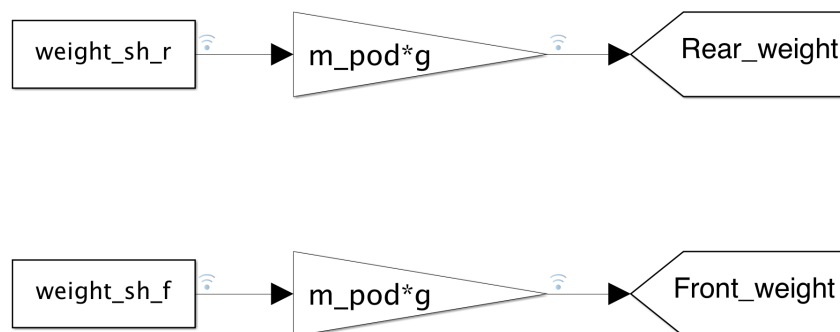


Figure 24: Blocks used to find the weight distribution on the front and rear wheels

Section 4. Pod Analysis

4.4.2 Front Wheel

The underlying equation for the loop shown in Figure 25 is the equation of motion of a mass on a linear spring and damper system.

$$m\ddot{x} + c\dot{x} + kx = 0 \quad (41)$$

Where m is the mass of the pod, c is the damping constant, k is the spring constant and x is the displacement of the wheel.

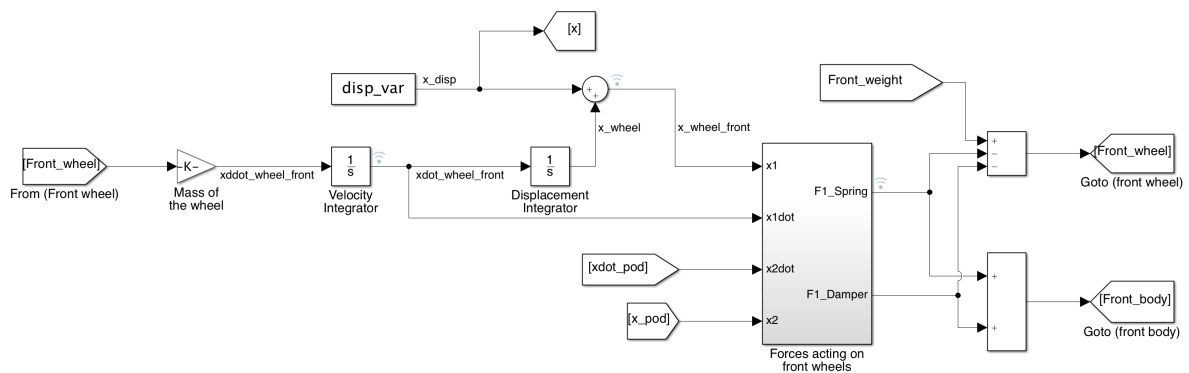


Figure 25: Loop of the Simulink blocks used to find the forces on the front wheels

Following the blocks from left to right beginning at the "Front_wheel" starts the loop with the force from the previous time step (initially set to zero). This is then divided by the mass of the wheel by passing through the gain block with a value of $\frac{1}{\text{mass of wheel}}$. This now passes to the first integrator where the signal is converted to a velocity.

At this stage the signal splits into two. One part leads to the force block where the forces due to the suspension system on the pod are resolved, while the other passes through the second integrator - converting the signal into a displacement. Now that the signal is a displacement, the change in vertical height from the track generator can now be added to the signal as a disturbance. This method does not restrict the vertical movement of the wheel and permits the expected overshoot from the rapid accelerations caused by the wheel going over a bump to occur.

The first subsystem in the loop (shown as a grey rectangle) resolves the forces that act on the front part of the pod. It outputs the forces caused by the spring and dampers by taking four inputs that are affected by track irregularities:

Section 4. Pod Analysis

1. Vertical wheel displacement
2. Vertical wheel velocity
3. Net vertical velocity of the pod
4. Net vertical displacement of the pod

The blocks inside of this subsystem describing the functions of the input and output are shown in Figure 26. The numbered blocks represent the block inputs mentioned above.

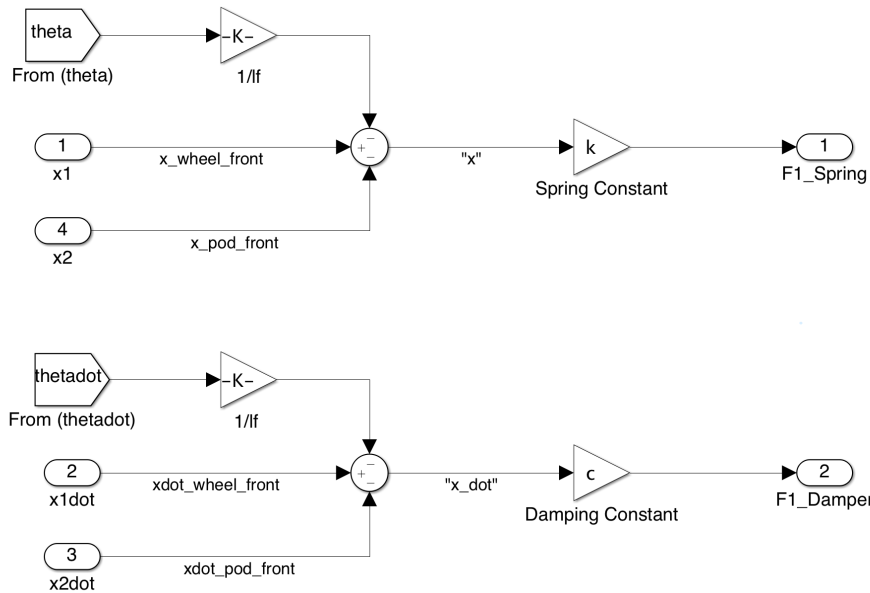


Figure 26: Contents of the force subsystem in the front wheel loop

Further to the inputs on the block itself, the subsystem also takes the outputs from the moment loops and calculates the moment about the centre of the pod to the contact point of the wheel - for both angular velocity and displacement. The spring forces are calculated using Hooke's law by the equation:

$$F = -kx \quad (42)$$

Where x is the total extension of the spring which connects the pod to the wheel, given by $x = x_{wheel} - x_{pod} - L_{front} \times \sin(\theta)$ and $\sin(\theta) \approx \theta$ by the small angle approximation. Although the suspension wheels are on a rocker system, this is modelled as a linear connection for the sake of simplicity. The resultant forces can then be scaled by the appropriate rocker ratios to the appropriate mounting points on the module.

Section 4. Pod Analysis

Passing this x value through the spring constant multiplier then gives the resultant force on a spring of a given spring constant caused by a disturbance in the track.

In a similar fashion, the force on the wheel caused by the damper is found using:

$$F = -c\dot{x} \quad (43)$$

And the resultant force is found by subtracting the relative angular and absolute vertical velocity of the pod.

Finally, there are two adders after the force subsystem which sum and subtract the forces exiting the block. The subtracted forces are fed back into the front wheel loop again, while the summed forces go to the moment loop to calculate the pitch of the pod.

Both of these adders are required because the model follows the convention when upwards is the positive direction. Therefore, when there is a positive displacement, there is a negative force on the wheel expected by equations 42 and 43. Since the force at the other end of the spring is equal and opposite to the force on the wheel (assuming no losses) the total force on the body of the pod is therefore positive.

4.4.3 Rear Wheel

This loop is very similar to the front wheel loop in every way. The only difference is that there is a time delay on the input from the track generator. This is calculated before the simulation is ran and passed to Simulink at the same time as the track and is equal to the expected time difference of the front wheel and rear wheel hitting a bump, expressed as:

$$t_{delay} = \frac{L_{mod}}{v_{pod}} \quad (44)$$

Where L_{mod} is the distance between the suspension modules and v_{pod} is the current speed of the pod. This part of the model is shown in Figure 27.

Section 4. Pod Analysis

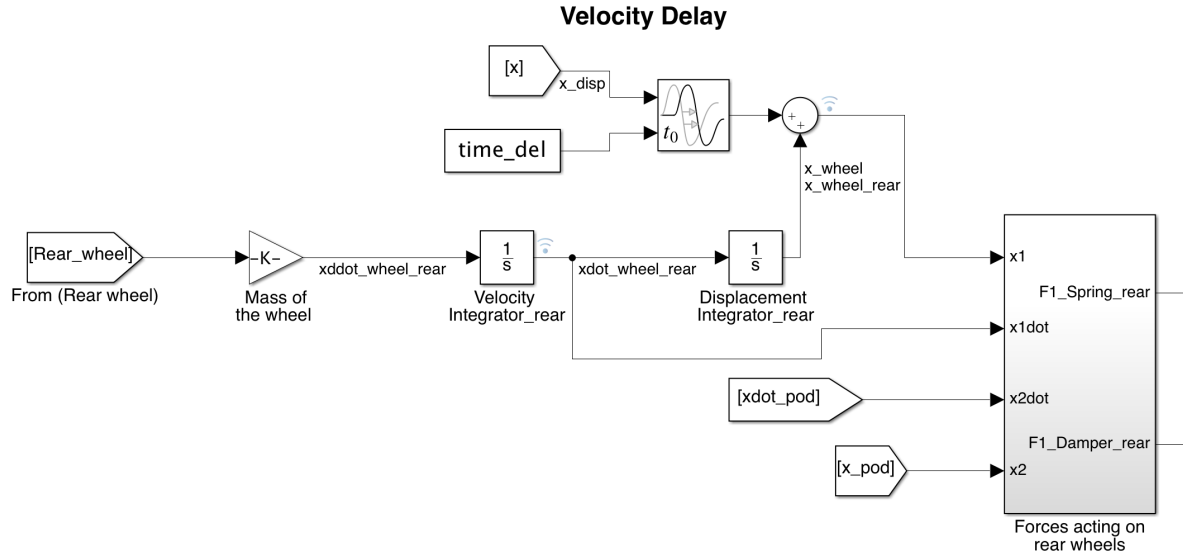


Figure 27: Loop of the Simulink blocks used to find the forces on the rear wheels

4.4.4 Moment

This part of the model is a forward loop that models the angular behaviour of the pod by taking the outputs from the two suspension modules and finds moments about the centre of the pod to find rotational displacement and velocity. These results are then fed back into the system for the front and rear modules, shown in Figure 28.

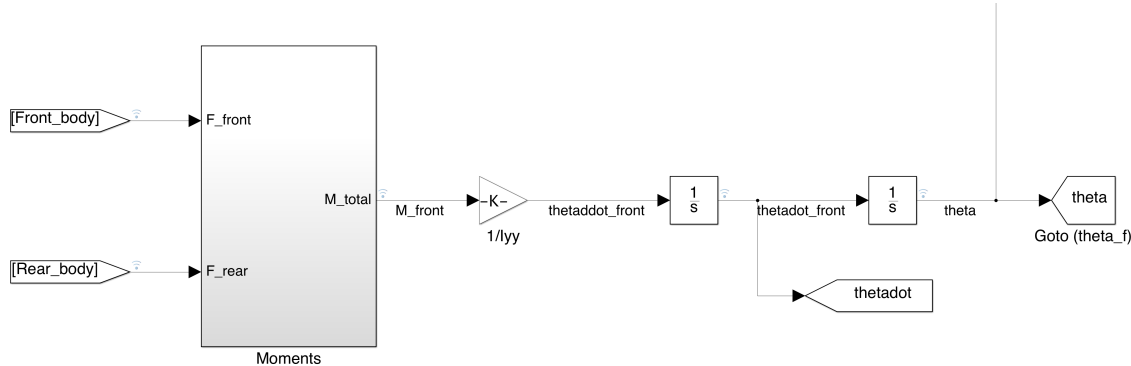


Figure 28: Loop in the Simulink model used to find the angular movement of the pod

The subsystem here takes the summed force on the front and rear suspension modules and outputs the total moment - or torque - about the centre of the pod. Figure 29 shows

Section 4. Pod Analysis

the contents of this subsystem. It is a simple moment balance where a positive moment is anti-clockwise and a negative moment is clockwise.

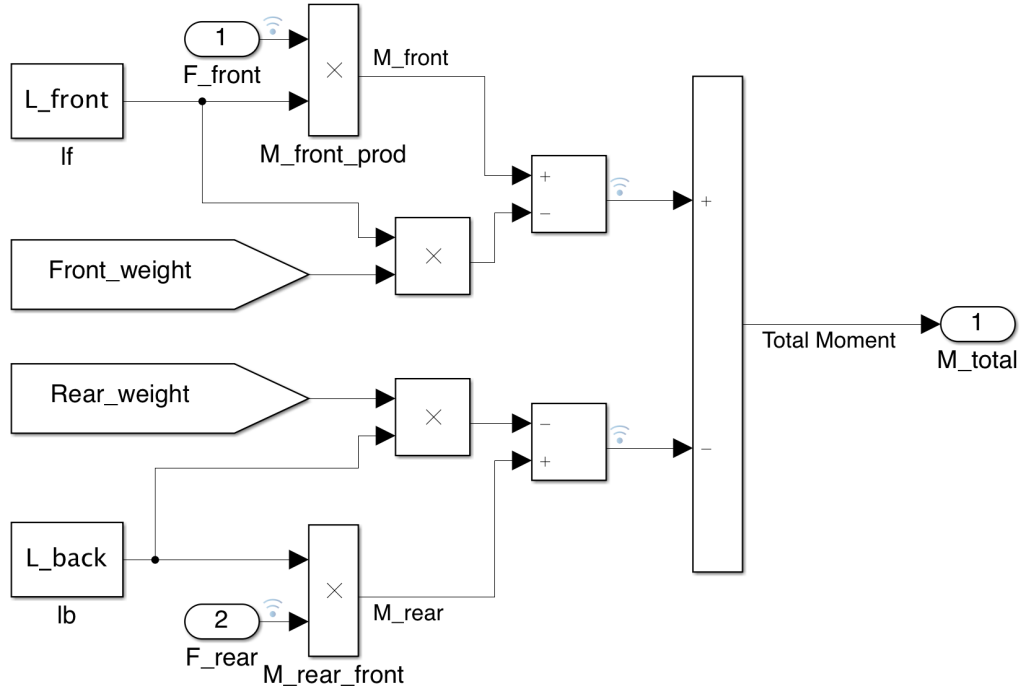


Figure 29: Contents of the moment subsystem

The moments are calculated in the form of $\sum M = \sum Fx$ where F is the force on the front and rear wheels, and x is the distance from the centre to either the front or rear suspension module. To fit the coordinate system, the disturbance from the front wheel is added, while the disturbance from the rear wheel is subtracted from the total moment.

Following Newton's Second Law for angular rotation:

$$\tau = I_{yy}\alpha \quad (45)$$

Where τ is the moment about the centre of the pod, I_{yy} is the moment of inertia along the length of the pod, and α is the angular acceleration of the pod. Therefore the angular acceleration can be calculated by dividing the moment outputs from the block by the moment of inertia. Passing this signal through an integration block gives the angular velocity, and a further integration block gives the angular displacement of the pod.

Section 4. Pod Analysis

4.4.5 Bounce

The final loop in the model is used to find the vertical movement of the pod about its centre of mass. This is a simple loop that sums the forces on the suspension modules described earlier. Figure 30 shows this process.

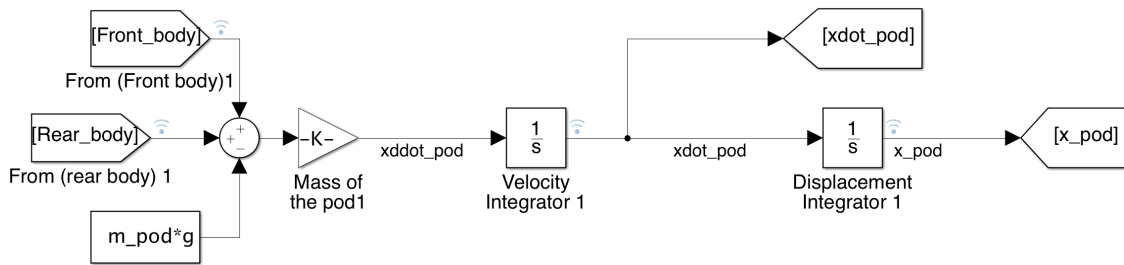


Figure 30: Loop in Simulink model used to calculate the absolute vertical movement of the pod

First the forces are summed, then divided by the mass of the pod to find the vertical accelerations. Next this acceleration is passed through an integrator to find the vertical velocity, followed by another integrator for the absolute vertical displacement. Both of these signals are tapped and sent back to the loops characterising the suspension modules.

4.4.6 Output

All of these blocks loop over the time-steps and disturbances from the track generator, are displayed on a scope and saved to the Matlab work-space so that various iterations can be run, adjusting the suspension parameters each time. The following figures show the output from the model with a spring constant of $k=50,000$ and damping constant of $c=100$.

To verify that the output of the model was correct, a flat track configuration was made with no disturbances. Figure 31 shows the displacement of the front wheel following the equation $x = F/k$, with an average of 0.029m. Figure 32 shows the average force on the front body being approximately half the weight of the pod at 1471N.

The variance in these values also confirms the correct operation of the weight transfer block - starting lower during acceleration when most of the weight is transferred to the rear wheels and increasing when the pod is decelerating and the weight is transferred to the front wheels. The output for the rear wheels was similar but showed the force and displacements decreasing during braking as expected.

Section 4. Pod Analysis

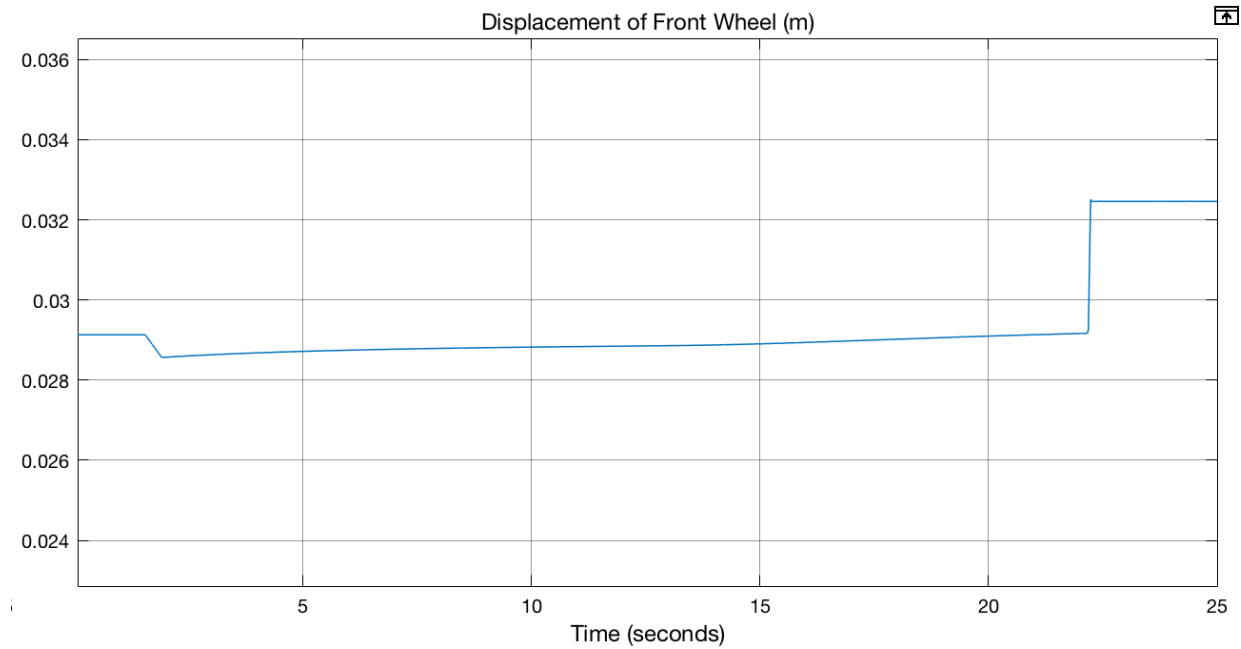


Figure 31: Output from Simulink model confirming the wheel displacement is output correctly

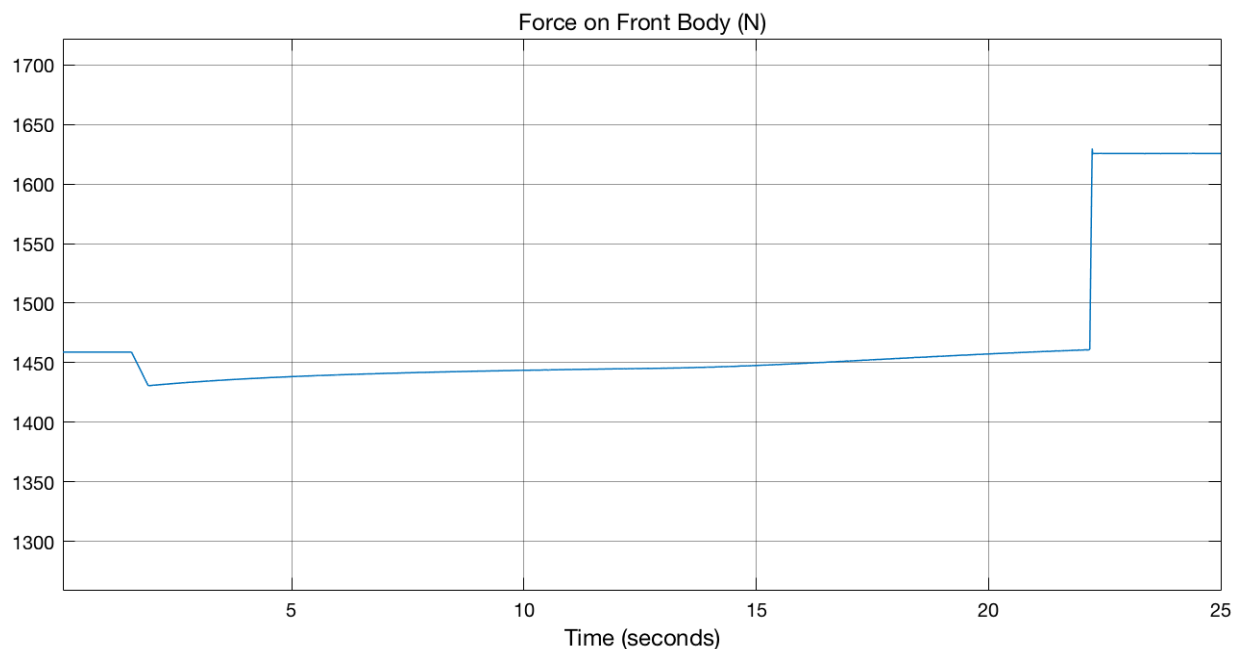


Figure 32: Output from Simulink model confirming the force is output correctly

Now applying an uneven track configuration gives the maximum displacements of the wheel and maximum forces exerted on the body of the pod. Figure 33 shows the displacement variation is between 1-2mm and Figure 34 shows the force variation is around 60N.

Section 4. Pod Analysis

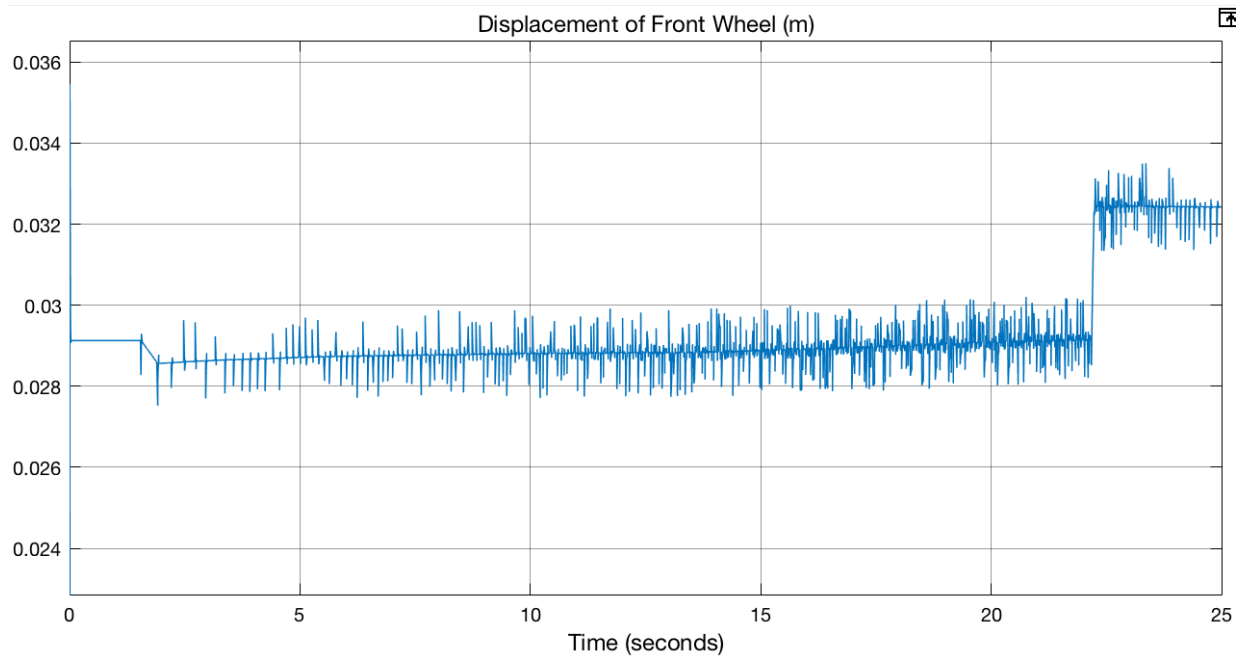


Figure 33: Output from Simulink model showing the front wheel displacement during a run

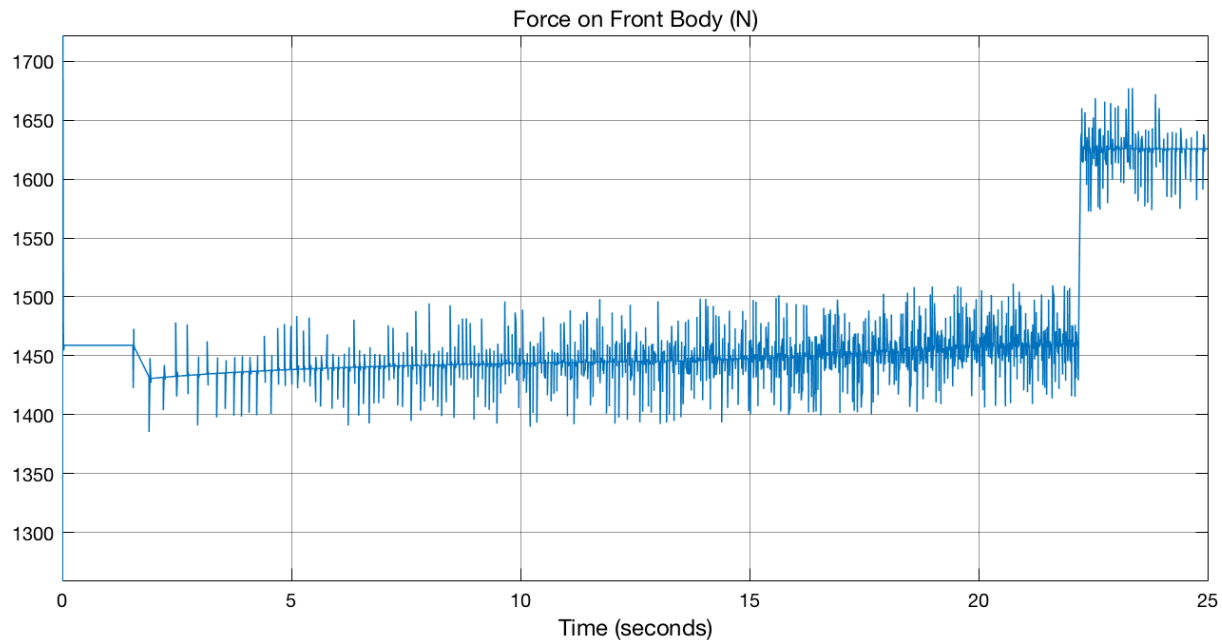


Figure 34: Output from Simulink model showing the force on front body during a run

4.5 Optimisation

4.5.1 Values to Avoid

A critical part of choosing suspension parameter is avoiding exciting the contact points at the resonance frequency. This becomes difficult in this case since the forcing frequency varies proportionally with the pod's current speed.

This is due to the force transmission to a structure varying with the ratio of the natural frequency to the excited frequency. As previously mentioned, the transmissibility ratio (TR) equation is:

$$TR = \sqrt{\frac{1 + (2\zeta r)^2}{(1 - r^2)^2 + (2\zeta r)^2}} \quad (46)$$

Where r is the frequency ratio (excitation/natural) and ζ is the damping ratio. Figure 35 shows how the frequency transmitted to the pod varies with the frequency ratio when $k = 50,000$ and $c = 100$.

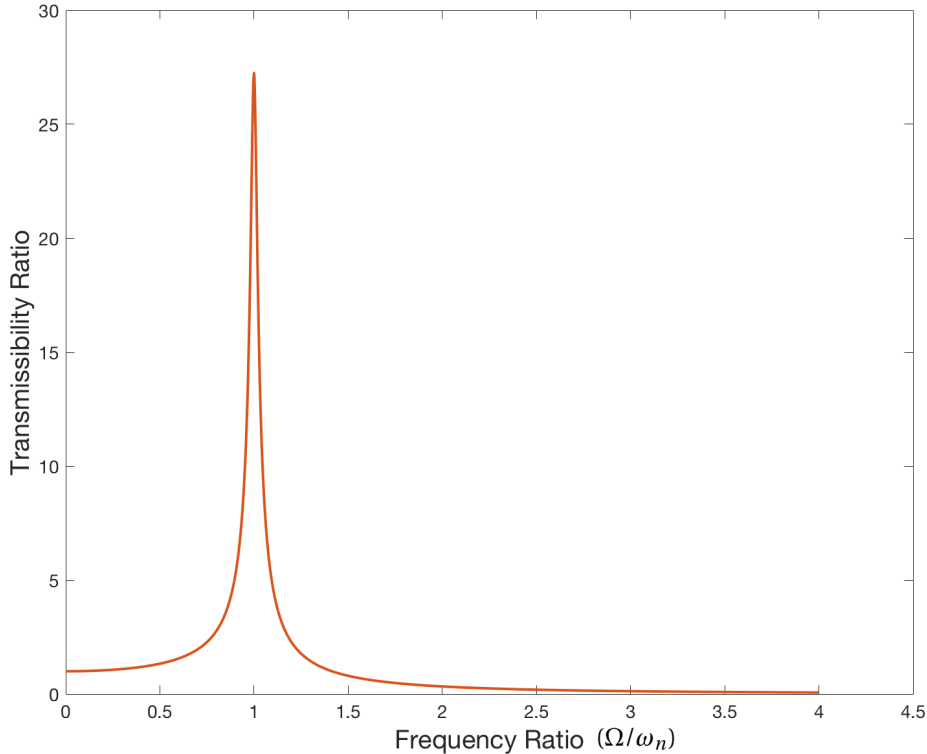


Figure 35: Natural frequencies of pod at a range of spring constants

Section 4. Pod Analysis

It is clear from this figure that the pod would benefit from a natural frequency several times lower than the frequency of bumps in the track. When $r = 1$ the TR is almost 28 while when $r = 3$ the TR is close to 0.1. Therefore, it is important that r is as high as possible when travelling at high velocities.

In order to find an appropriate range of k values, the natural frequencies for a range of spring constants from 100 - 500,000N/m was plot (Figure 36) with a constant c of 100Ns/m since damping has no effect on the undamped natural frequency. The horizontal lines on the figure represent the forced frequencies from track irregularities at 1/2, 1/4 and 1/8 of the top speed (90m/s).

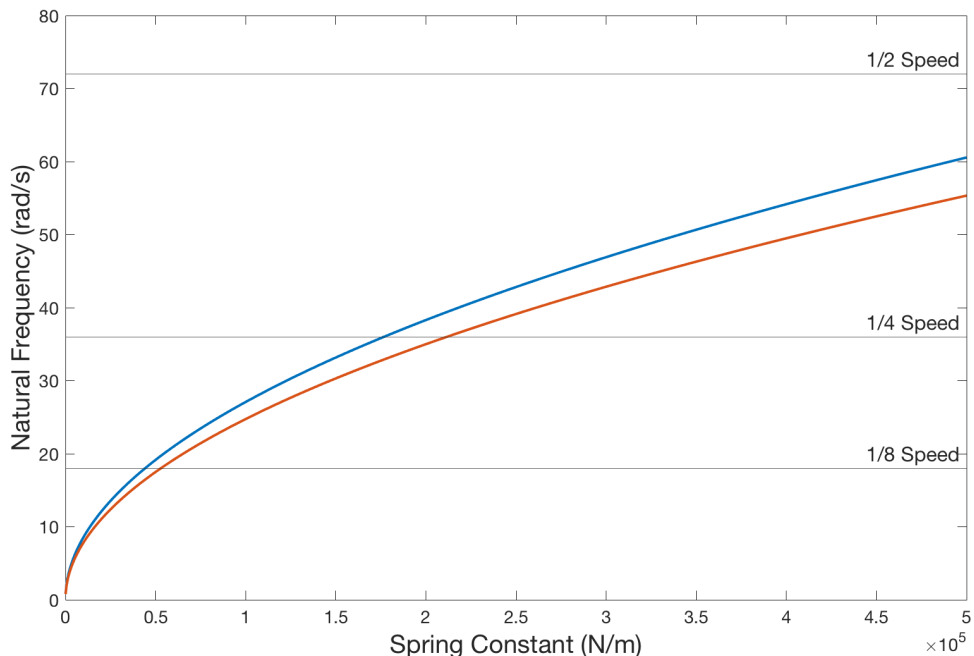


Figure 36: Natural frequencies of pod at a range of spring constants

Choosing a spring constant below 100,000N/m ensures that the natural frequency is under 25rad/s and the resonant frequency is experienced at a low speed. A forcing frequency of 25rad/s occurs when the pod is travelling at 15m/s, around 2.6 seconds after pulling away from the starting line, only having experienced five bumps in the track. This means that there will be a high frequency ratio for the majority of the run, only briefly passing the resonance frequency again for under 0.27s when braking.

5 Test Rig

5.1 Concept

Reproducing the vibration environment is a very useful tool to test various components on the pod. Ideally the whole system would be tested and mounted onto a section of track and tested. However, a rig of this scale would be a very expensive and time consuming project to execute safely, whose assembly is beyond the scope of this research.

Therefore, a small scale test rig has been manufactured and a concept full scale rig has been designed to be carried on as a future project.

5.2 Small Scale System Design

As a proof of concept, a small test rig 250mm in height was designed and manufactured. The frame of this system is made with aluminium profiles, providing an easily adjustable rigid structure with an aluminium plate attached to the top that is free to move in the vertical direction but is constrained laterally. An eccentric mass driven by a synchronous motor is fixed to the underside of this plate to provide the forcing frequency.

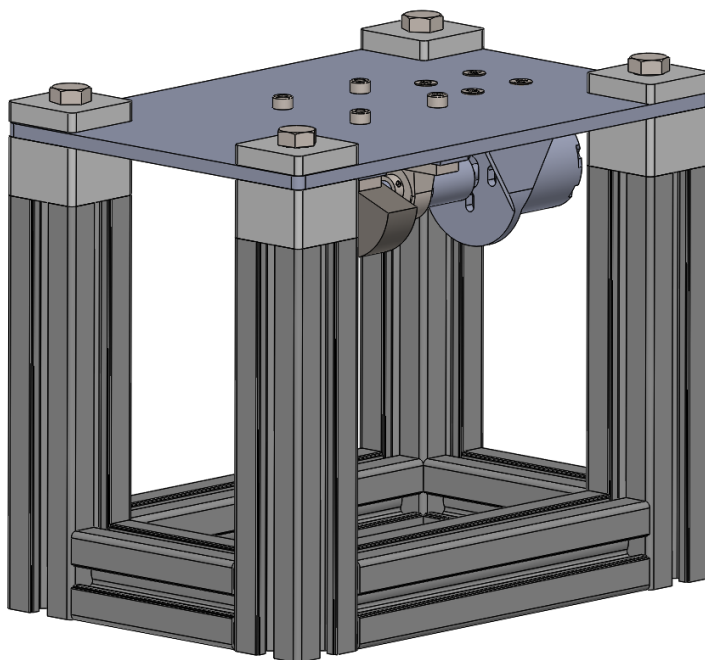


Figure 37: 3D model of the small scale test rig

Section 5. Test Rig

While the low budget of the project contributed to some of the design choices that were made, there were several considerations that constrained the design of system:

- Constraining lateral movement
- Damping the vibrations transmitted to the support
- Accounting for any misalignment between the motor shaft and shaft of the ERM
- Taking the eccentric load off the shaft of the ERM to prevent damage to the motor

To constrain the lateral movement, the aluminium profiles in the corners were tapped and the plate was fixed in four corners using M12 bolts going through the plate. Between these sections there were two foam blocks to damp the vibrations in which the bolt was inserted into an oversized through hole (14mm) shown in Figure 37 .

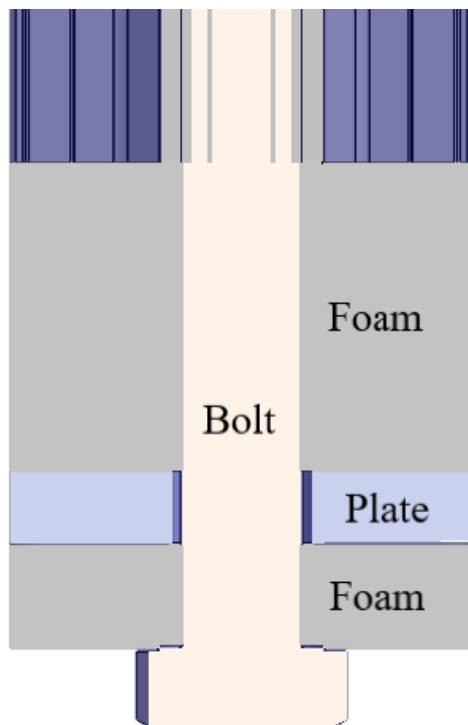


Figure 38: Mechanism to reduce the lateral movement of the plate

In order to deal with the shaft alignment a flexible shaft coupling was used, this allows for torque to be transmitted along the shaft even with a slight misalignment between the two.

Section 5. Test Rig

Finally, after the shaft coupling and enclosing the ERM were two pillow blocks to take the eccentric load which were then mounted onto aluminium spacers to give the ERM clearance to spin freely. Figure 39 shows a close up of this mechanism.

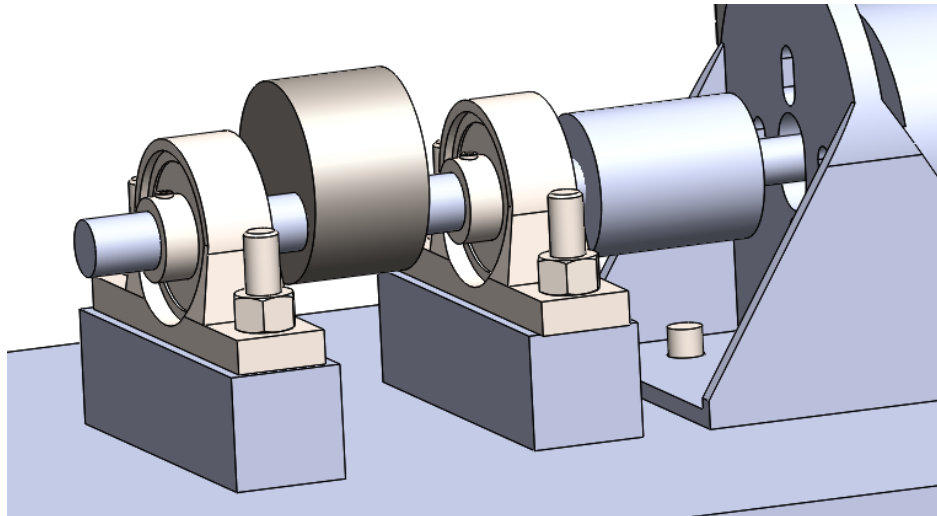


Figure 39: Mechanism used to take the load off of the motor shaft

For the electronics, a Raspberry Pi model 3 was used connected to an MPU-6050 three axis accelerometer and both were powered from a USB battery pack. This configuration was chosen so that SSH communication via Wi-Fi could be used - allowing the tests to be performed with no physical connections to the PC that could come loose or give erroneous readings.

The MPU-6050 was chosen for its compatibility with a Python based open source vibration monitoring software package that was designed for the Raspberry Pi called Vibe. A web-server runs on a paired computer, saves and analyses the data, while the readings are logged in batches on the Pi and then sent to the host PC.

The motor used was an APS 5065S 2.2kW permanent magnet synchronous motor paired with a Hobbywing Skywalker 2-6S 80A electronic speed controller (ESC). This ESC is rated for much higher power than what is required so that it could be run continuously with no concerns of overheating. Speed control was done manually with a potentiometer that would vary the duty cycle of a PWM signal going to the controller. A tachometer was used in conjunction with a piece of reflective tape on the motor to set the correct RPM before readings were taken from the IMU.

5.3 Small Scale System Implementation

The actual system followed the design mentioned in the previous section closely, with the only changes being to bolt sizes and the inclusion of the corner sections to give the structure rigidity. Figure 40 shows the full test rig shortly after assembly was completed.

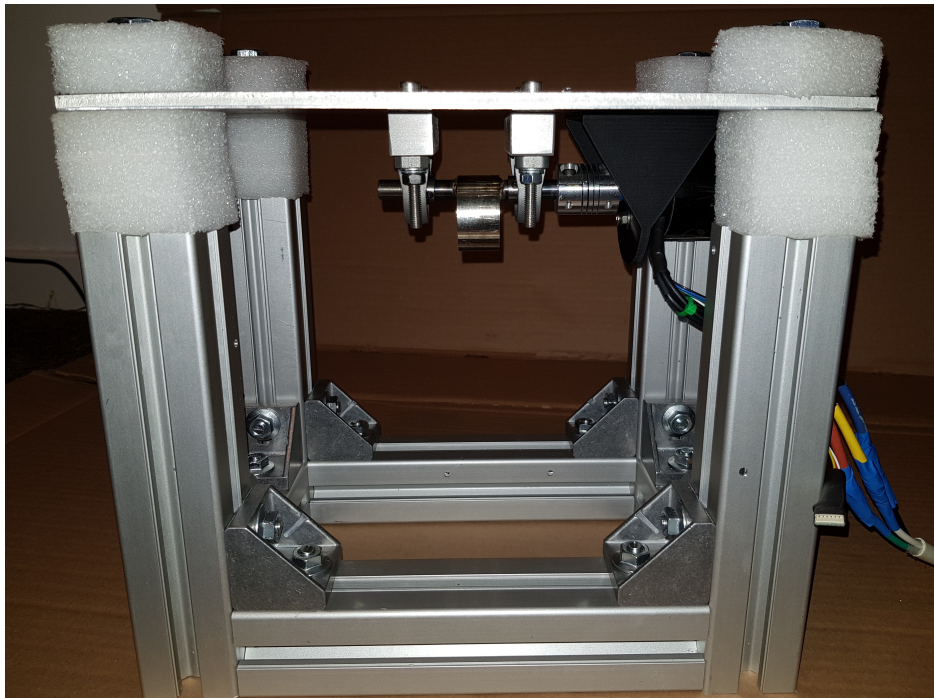


Figure 40: Side view of the finished test rig

The mechanism of the pillow blocks, spacers and flexible shaft coupling used to take the load off the shaft can clearly be seen here but a closer view is shown in Figure 41. It can also be seen that the ERM was weld onto the shaft to make sure it did not come loose during operation. Lastly, the full setup of the system including the power supply, ESC, Raspberry Pi, computer and test rig (clamped to the workbench) is shown in Figure 42. The test rig specifications are summarised in Table 3.

Table 3: Summary of the manufactured small scale test rig

Mass of vibrating plate	2.05kg
Mass of ERM	0.17kg
ERM material	Stainless steel
Eccentricity	11mm
ERM thickness	21mm
ERM diameter	38mm
Dimensions (L/B/H)	300/200/250mm

Section 5. Test Rig



Figure 41: Implemented mechanism used to take the load off of the motor shaft

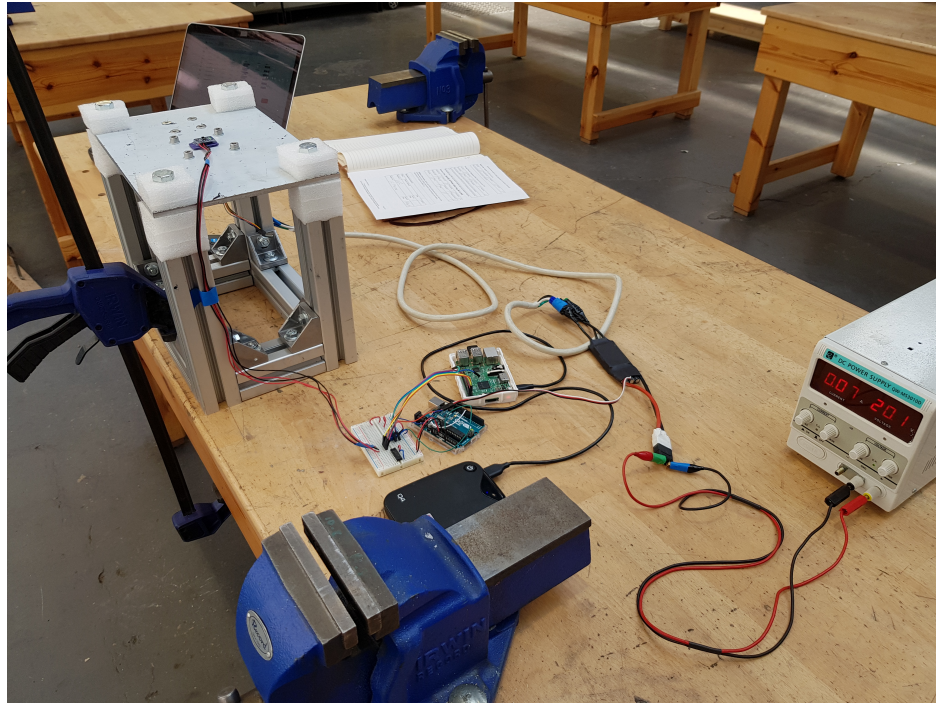


Figure 42: Full layout of equipment before experiment was carried out

5.4 Full Scale System Concept

Taking inspiration from the quarter car test rigs used in the automotive industry, a conceptual design for a modular half pod test rig has been made (shown in Figure 43). The working principle is that having the pod mounted onto two split sections of rail would most accurately excite the suspension in a similar manner as done in a quarter car test rig, with the front section moving slightly earlier than the rear as done in the Simulink model. This test rig operates in a very similar manner to the scale model but used a larger eccentric mass and features a modular attachment system to change the magnitude of the force transmitted to the top plate - where the rail would be attached. The small length of rail is designed as such to only fit a small portion of the pod.

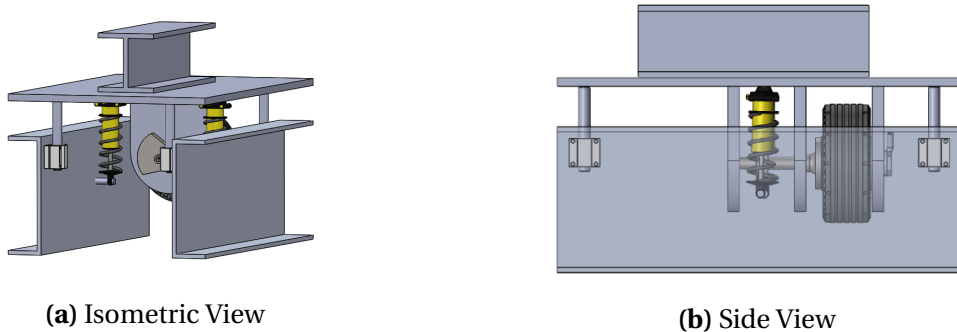


Figure 43: 3D model of half-pod test rig concept

Splitting the system into two separate sections provides much more freedom in the testing that can be performed on the pod components. Figure 44 shows two test rigs underneath the current 2019 pod. This creates more flexibility in the testing modes as three or even more systems could be aligned to test pods of many different designs.

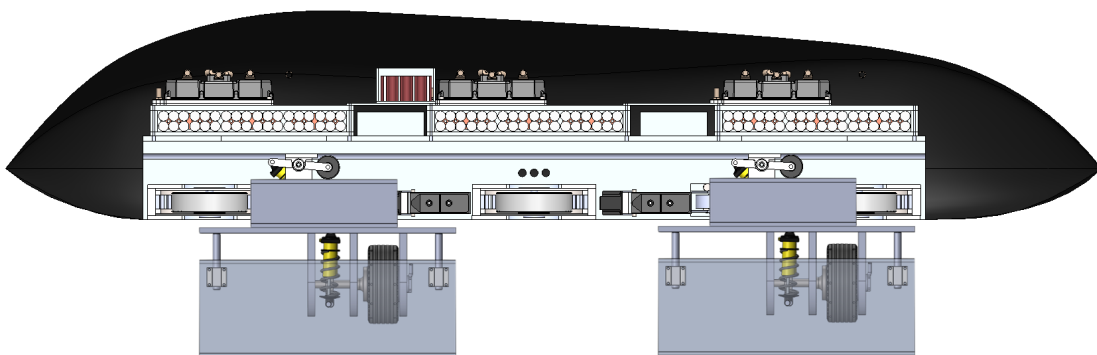


Figure 44: Cross section showing the possible arrangement of multiple test rigs to accommodate the current pod design

6 Results

The Vibe tool offers several features for analysis. It works by taking samples over a predefined period of time and saves them to the Raspberry Pi before sending them over to the host server where they can be analysed.

A baseline measurement was made before taking any measurements while the apparatus was running. This indicates the orientation of the accelerometer and its accuracy. Figure 45 shows the raw data from each axis of the accelerometer, clearly the Z axis represents the vertical direction since its value is 1g. From experimentation it was found that the Y axis is the axis tangential to the rotation of the mass and therefore the X axis can now be ignored.

This raw data is then passed through a low pass filter to isolate gravity from the measurements and finds the tilt of the sensor. Figure 46 shows these readings and confirms that the sensor is almost perfectly flat and therefore oriented in an appropriate way to use each axis for a different degree of freedom in the test rig.

Lastly, Figure 47 shows the vibration data from the accelerometer, which are the readings taken relative to the average orientation - therefore showing the absolute value of the vibrations. Since the system was at rest, it showed that the accuracy of the readings taken by the sensor is roughly $\pm 0.01g$.

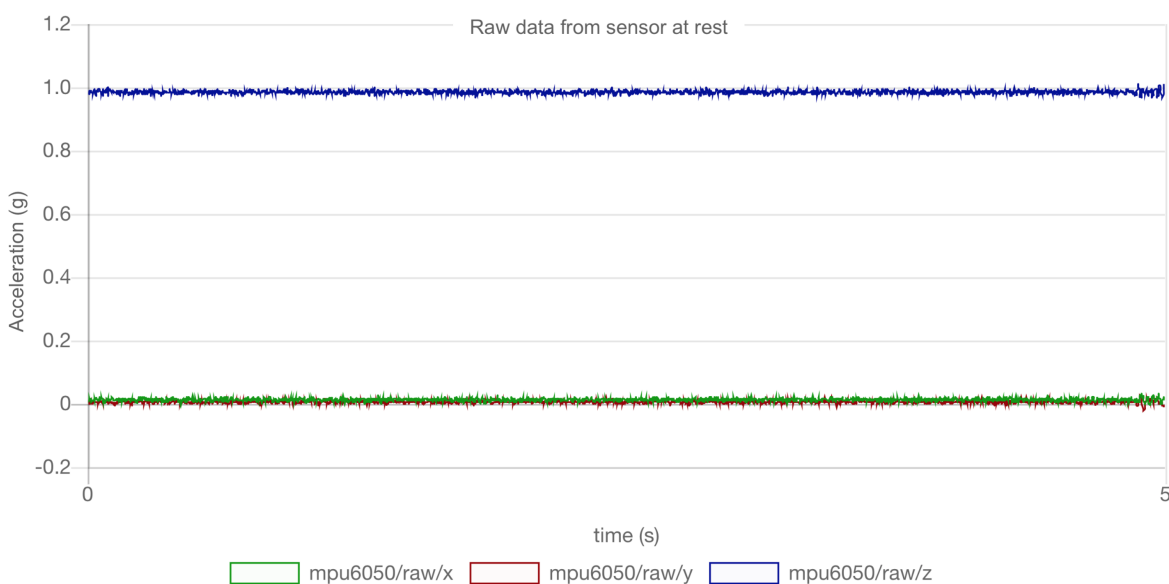


Figure 45: Raw data from accelerometer at rest

Section 6. Results

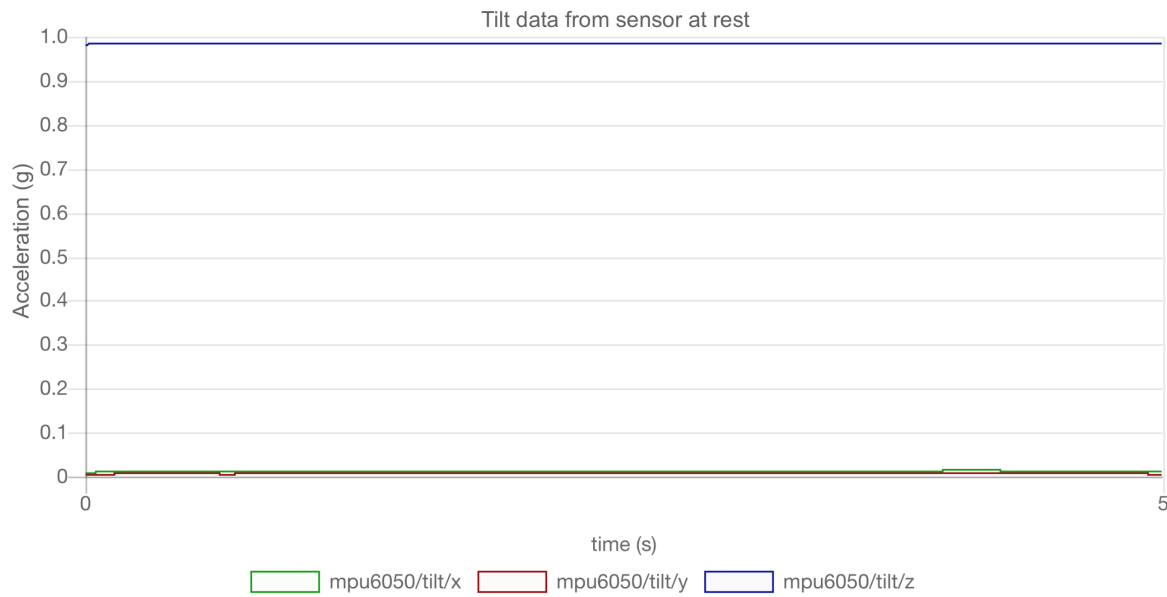


Figure 46: Low-pass filtered tilt data from the accelerometer at rest



Figure 47: Vibration data from accelerometer at rest

Section 6. Results

6.1 First Batch

Five samples lasting five seconds each were taken over a range of forcing frequencies by changing the RPM of the motor. The average value from the peaks of the readings were taken and are shown in Table 4, and Figure 48 shows the force transmitted to the vibrating plate in the Y and Z axes. The values of force are found with Newtons first law ($F = ma$), where the mass of the vibrating plate is 2.05kg.

Table 4: First Batch of Measured Values

RPM	Pod Speed (m/s)	Z accel (g)	Y accel (g)	Z force (N)	Y force (N)
500	31.67	0.1446	0.2096	2.9079	4.2151
600	38	0.2678	0.3429	5.3855	6.8958
745	12.42	0.312	0.6184	6.2744	12.4363
810	31.5	0.5126	1.0258	10.3086	20.6293

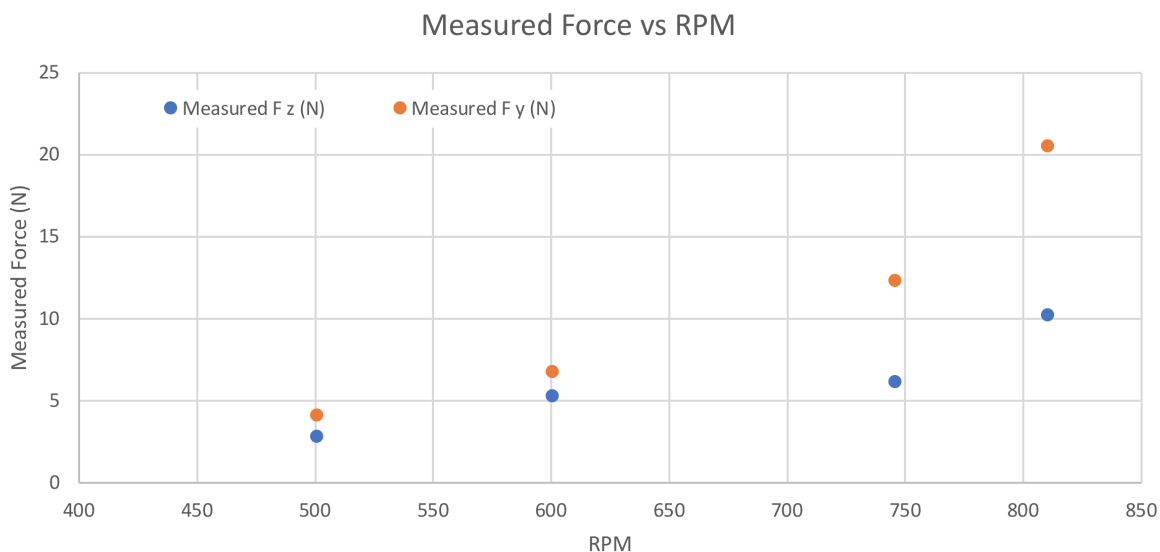


Figure 48: Force vs RPM from first batch of readings

These values immediately raised concerns since the forces in the Y axis were much larger than in the X axis. Additionally, after reaching 800rpm, the test rig was making a loud rattling sound and the experiment was stopped due to safety concerns. The top vibrating plate was not secured enough and was sliding between the foam blocks, hitting the bolts that were keeping it in place. These impacts were causing the rattling noise and were recorded by the data logger shown in Figure 49.

Section 6. Results

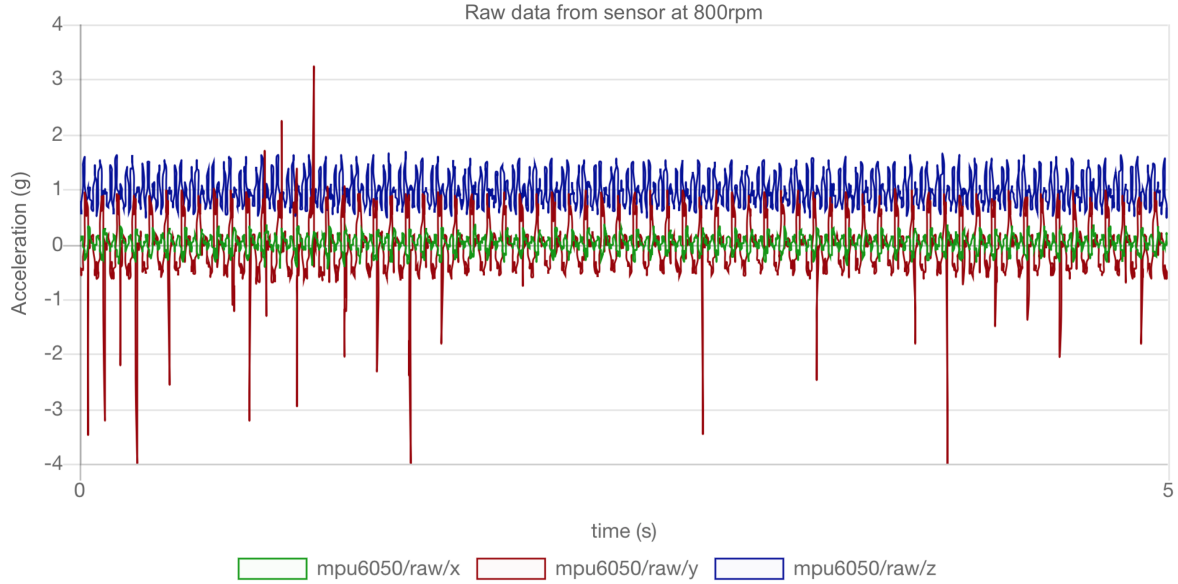


Figure 49: Raw data from accelerometer at 800rpm during first test

The large spikes in the data from the Y axis readings (up to 4g) confirmed the flaw with the test rig. It was then modified by using shorter bolts and large washers that compressed the foam blocks more, allowing it to go to higher speeds.

6.2 Second Batch

After making the modifications, the following results shown in table 5 were recorded. Although the forces at higher rotational speeds are still larger in the y axis, there was no rattling noise during operation so the tests continued.

Table 5: Second batch of Measured Values

RPM	Pod Speed (m/s)	Z accel (g)	Y accel (g)	Z force (N)	Y force (N)
500	31.67	0.1736	0.1046	3.4911	2.1035
600	38	0.1392	0.1216	2.7993	2.4454
700	44.33	0.1406	0.1646	2.8275	3.3101
800	50.67	0.194	0.1678	3.901	3.3745
900	57	0.1972	0.2944	3.9657	5.9205
1000	63.33	0.283	0.7288	5.6912	14.6565
1120	70.93	0.4672	1.2824	9.3956	25.7897
1255	79.48	0.677	2.2302	13.6148	44.8504

Section 6. Results

The results follow a much more controlled pattern compared to before although the readings are much lower. This was the expected outcome since there was less compliance in the foam and therefore less movement. The measured force plot against the rpm the measurement was taken at is shown in Figure 50.

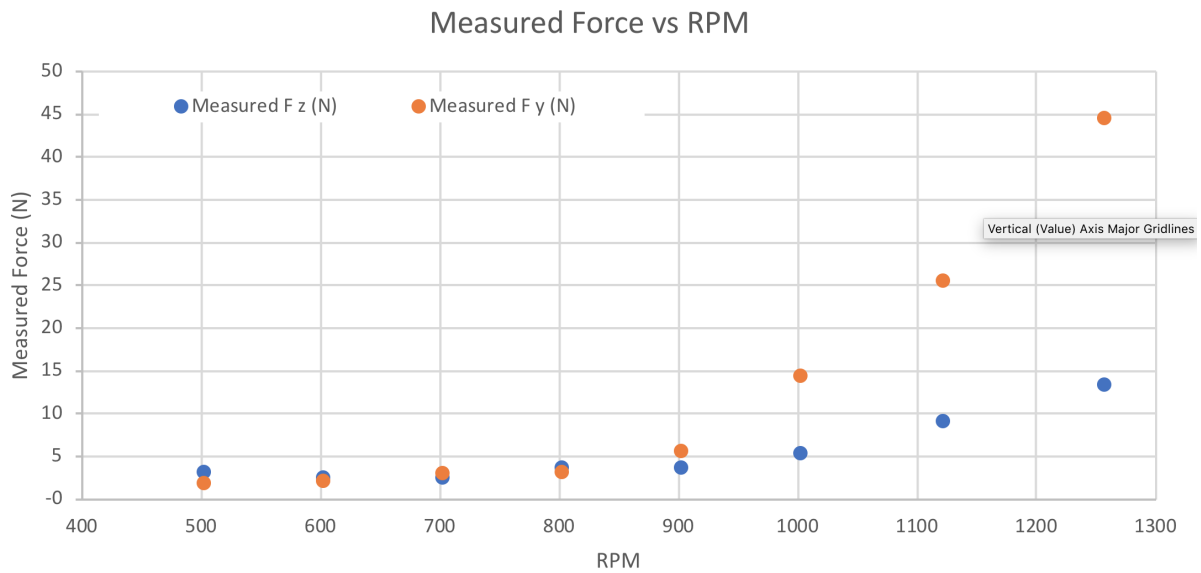


Figure 50: Force vs RPM from second batch of readings

Despite this being a small scale test rig, the force readings in the Y axis of around 45N came closer than expected to the expected force on the wheels of the pod of around 60N depending on the track configuration.

The theoretical force from the ERM was then calculated using the equation mentioned earlier:

$$F = mew^2 \quad (47)$$

Allowing the transmissibility ratio for the Y and Z axis to be recorded, shown in table 6. This data was then plot in Figure 51.

Section 6. Results

Table 6: Theoretical Force and transmissibility ratio in y and z axes

RPM	ERM Force (N)	TR (z)	TR (y)
500	5.126711175	0.68097	0.4103
600	7.382464092	0.3791	0.3312
700	10.0483539	0.28139	0.3294
800	13.12438061	0.2972	0.2571
900	16.61054421	0.23875	0.3564
1000	20.5068447	0.27753	0.7147
1120	25.72378599	0.36525	1.0025
1255	32.29879307	0.4215	1.3886

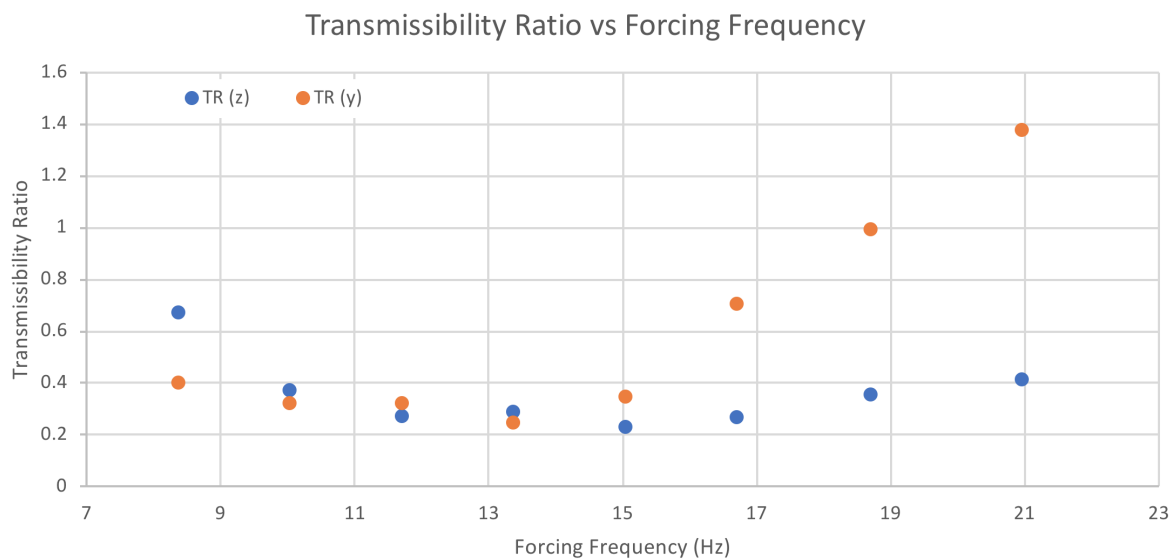


Figure 51: Transmissibility ratio at different forcing frequencies

There is a clear positive parabola in these results which suggests that the natural frequencies of the foam lie below 7Hz and above 21Hz. However this range of data is not large enough to confidently assume this to be true.

The test rig successfully created a vibration environment that could be used to test components such as the electronics in harsh conditions and the suspension to a limited degree. However, there is room for improvement in both the rig and the tests that were carried out.

Section 6. Results

6.3 Possible Improvements

More accurate and predictable results could have been obtained if the testing procedure and aspects of the rig design were changed.

The most important change to the rig would be to use linear bearings instead of the bolts in an oversized hole keeping the plate in place with the friction of the foam block. Furthermore, the foam blocks should not have been the main form of transmitting force to the plate. Using a linear spring and damper system would have allowed the transmitted force to be predicted so that a specification of force values at a given rotational speed could be made.

With regards to the testing procedure, if the entire rig was secured to a structure that was more rigid than the workbenches in the lab, the results would be more clear and disturbances would be isolated. The entire bench was vibrating when running at high speed which was detected by the accelerometer. Figure 52 shows the measured x value being almost as large as the measured z value ($0.609g$) despite no forces from the ERM directly acting on this degree of freedom.

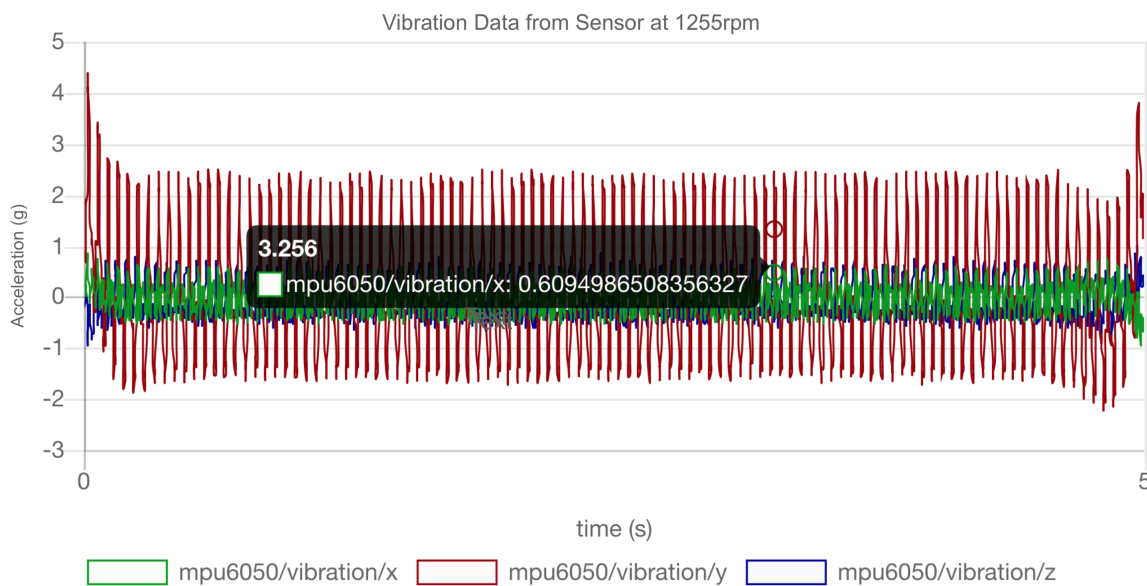


Figure 52: Data from sensor at high RPM showing the noise caused by the vibrating workbench

Finally, if a closed loop system was used to measure the RPM and then adjust the output from the ESC to match a desired speed, the forcing frequency could be accurately varied with time to match the output of the track generator. Giving a true representation of the vibration environment of the test track.

7 Conclusions

All six of the key objectives of this project that were set out in the beginning were completed and there is now a solid foundation for future teams to model their new suspension designs. All of the scripts and models are fully adjustable so any changes to the pod can be accounted for. The track generator could even be modified in the unlikely event that the track changes or if the disturbances of another vehicle - for example a train - travelling over varying steps and gaps of a known size is to be modelled.

Future work would be to expand on the models to find the response of the pod in more degrees of freedom. The assumption was made that lateral and roll forces were negligible in comparison but these are not zero. Furthermore, the accuracy of the model would increase if the acceleration forces were localised to their accurate location on the pod and if velocity was not conserved when travelling over a bump.

Despite the test rig not providing results as accurate as were hoped for, it still created a vibration environment similar to that of the pod during a test run that could be analysed and used for testing. The issues with the design are known and can therefore be improved on in a future iteration. A positive aspect to take from this is that that vibrations are in multiple directions so tests on components would be more strenuous and give a harsher vibration environment than what is expected.

Future work on the test rig would be to improve the current design, constraining lateral movement and using a more controlled means of force transmission. A closed loop system monitoring the motor speed and varying it in accordance with the output from the track generator would also give much more accurate results. Or with a larger budget, hydraulic actuators could be used to give a more controlled excitation force similar to what is done in industry. Furthermore, the half-pod test rig could be manufactured to test the system as a whole rather than the individual components.

References

- [1] Stephenson J. Clayton G.A. Morland G.W. Jenkins, H.H. and D Lyon. The effect of track and vehicle parameters on wheel/rail vertical dynamic forces. *Railway Engineering Journal*, 1974.
- [2] J. H. Kuang Y. C. Chen. Modelling of wheels and rail discontinuities in dynamic wheel-rail contact analysis. *Department of Vehicle Engineering, National Pingtung University of Science and Technology*, pages 265–273, 2002.
- [3] Tribonet. Hertzian contact theory. <http://www.tribonet.org/wiki/hertz-contact-theory/>, 2017. Online; accessed 29th of January 2019.
- [4] Michael J. M. M. Steenbergen. Modelling of wheels and rail discontinuities in dynamic wheel-rail contact analysis. *International Journal of Vehicle Mechanics and Mobility*, Vol. 44:766–787, 2006.
- [5] Singiresu S. Rao. *Mechanical Vibrations, Fifth Edition*. Prentice Hall, Upper Saddle River, NJ, 2011.
- [6] S. Graham Kelly. *Mechanical Vibrations, Theory and Applications, SI*. Global Engineering, Stamford, CT, 2012.
- [7] Karl Berntorp. Derivation of a six degrees-of-freedom ground-vehicle model for automotive applications. *Lund University, Department of Automatic Control*, 2013.
- [8] Christoffer Routledge Anton Albinsson. The damper levels influence on vehicle roll, pitch, bounce and cornering behaviour of passenger vehicles. *MasterâŽs Thesis in Automotive Engineering, A study in cooperation with Volvo Car Corporation*, 2013.
- [9] Wisama Khalil Maxime Gautier Philippe Bodson Gentiane Venture, Pierre-Jean Ripert. Modelling and identification of passenger car dynamics using robotics formalism. *HAL*, 2009.
- [10] Salim Haidar Ali Mohammadzadeh. Analysis and design of vehicle suspension system using matlab and simulink. *Grand Valley State University*, 2006.
- [11] E. J. Lavernia J. Zhang, R. J. Perez. Documentation of damping capacity of metallic, ceramic and metal-matrix composite materials. *Materials Science and Engineering Department of Mechanical and Aerospace Engineering, University of California*, 1993.

Section References

- [12] Popular materials used for springs. <https://www.acxesspring.com/popular-materials-used-for-springs.html>, Published Date Unknown. Online; accessed 5th of February 2019.
- [13] F. Orban. Damping of materials and members in structures. *Journal of Physics: Conference Series*, 2011.
- [14] Steve Southward Corina Sandu, Erik R. Andersen. Multibody dynamics modelling and system identification of a quarter-car test rig with mcpherson strut suspension. *Vehicle System Dynamics International Journal of Vehicle Mechanics and Mobility*, Vol. 49:153–179, 2011.
- [15] Paul Sas Christophe Lauwers, Jan Swevers. Robust linear control of an active suspension on a quarter car test-rig. *Control Engineering Practice* 13, pages 577–568, 2005.
- [16] Lansmont. Model 1000 vibration test system. <http://www.lansmont.com/products/vibration/vertical/lansmont-standard-1000/>, Published Date Unknown. Online; accessed 10th of February 2019.
- [17] Space Exploration Technologies Corp. *SpaceX Hyperloop Pod Competition Rules and Requirements*, Vol. 4:18–21, 2019.